JOURNAL OF PETROLOGY | VOLUME 37 | NUMBER 1 | PAGES 117–143 | 1996

T. E. SMITH[1]*, M. F. THIRLWALL[2] AND C. MACPHERSON[2]
[1]DEPARTMENT OF GEOLOGY, UNIVERSITY OF WINDSOR, WINDSOR, ONT., CANADA N9B 3P4
[2]DEPARTMENT OF GEOLOGY, ROYAL HOLLOWAY, UNIVERSITY OF LONDON, EGHAM TW20 0EX, UK

Trace Element and Isotope Geochemistry of the Volcanic Rocks of Bequia, Grenadine Islands, Lesser Antilles Arc: a Study of Subduction Enrichment and Intra-crustal Contamination

Pliocene volcanics on the island of Bequia comprise two interbedded suites of basalts and andesites. The isotopically homogeneous suite (IHS) has a limited range of Sr–Nd–Pb isotopes ($^{87}Sr/^{86}Sr$ 0·7040–0·7046, $^{143}Nd/^{144}Nd$ ~0·5130 and $^{206}Pb/^{204}Pb$ 19·36–19·51), and mantle-like $\delta^{18}O$ values (~5·5 in clinopyroxene). The isotopically diverse suite (IDS) is characterized by much wider ranges of radiogenic isotopes ($^{87}Sr/^{86}Sr$ 0·7048–0·7077, $^{143}Nd/^{144}Nd$ 0·5128–0·5123 and $^{206}Pb/^{204}Pb$ 19·7–20·2), in which all of the Sr and Pb ratios are higher and Nd ratios are lower than those of the IHS. The IDS is also characterized by high $\delta^{18}O$ values, up to 7·6 in clinopyroxene. The Sr and Pb isotope ratios are too high, and the Nd isotope ratios are too low in the IDS for any of these lavas to be derived from unmodified depleted mantle.

Both suites are petrologically very similar and their major element compositions and phenocryst contents suggest that they were formed largely by fractional crystallization of a hydrous tholeiitic melt at pressures <3 kbar. The isotopic ratios and enrichments in large ion lithophile elements (LILE), and to some extent light rare earth elements (LREE), as compared with mid-ocean ridge basalts (MORB), of the IHS lavas suggest that they were derived from a depleted mantle source which had been re-enriched by the addition of 1–4% of a subduction component. This component probably comprised a mixture of dehydration fluids, and perhaps minor siliceous melts, released from subducting sediments and mafic crust. The extreme isotopic ranges, large enrichments in incompatible elements, more fractionated LREE patterns and higher $\delta^{18}O$ values of the IDS lavas are interpreted as resulting from ~10–55% assimilation–fractional crystallization of sediments, derived from the Guyana Shield, which are present in the arc crust, by IHS type melts.

KEY WORDS: *trace elements; radiogenic isotopes; arc lavas; Lesser Antilles*

INTRODUCTION

The island of Bequia lies in the southern section of the Lesser Antillean arc (Fig. 1), which formed along the eastern edge of the Caribbean Plate as a result of subduction of Jurassic to Cretaceous Atlantic Ocean lithosphere. The arc may be divided into pre-Miocene, Miocene and post-Miocene phases which are superimposed in the section of the arc south of Dominica.

Geologically, Bequia comprises mainly heterolithic debris flows, and other mass movement deposits, together with fluvial feldspathic sandstones, all of volcanogenic origin. The epiclastic sequences commonly contain coarse-grained plutonic blocks, composed mainly of plagioclase and amphibole. They are interbedded with mafic lavas and are cut by a few dykes trending mainly to the northwest. A few outcrops of monolithological ash flow, avalanche or crumble breccia deposits occur along the north coast. The sequence of coarse epiclastics, pyroclastics and lavas is interpreted as the proximal facies of the volcaniclastic apron developed on a marine strato-volcano (Cas & Wright, 1987). The lavas and dykes

*Corresponding author.

© Oxford University Press 1996

Downloaded from https://academic.oup.com/petrology/article/37/1/117/1530492 by guest on 21 August 2022

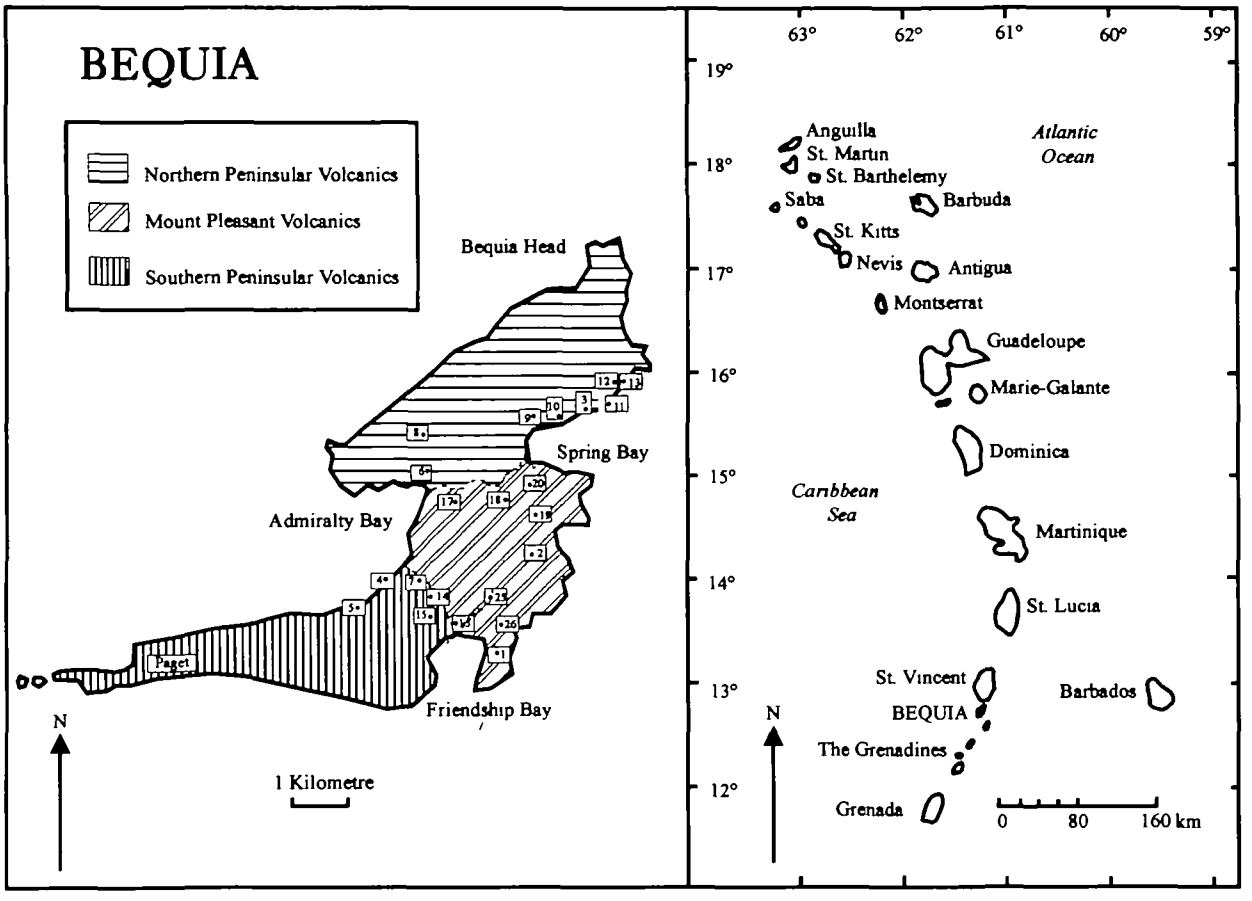

Fig. 1. Location of Bequia in the Lesser Antilles Arc, and sample localities.

described here were erupted or emplaced during the Pliocene (5·0–3·5 Ma) (Briden *et al.*, 1979). The sequence has been divided (Fig. 1) into the Southern Peninsular (~4·5 Ma), the Northern Peninsular (~4·5–3·5 Ma) and the Mount Pleasant (~5·0 Ma) formations (Westercamp *et al.*, 1985).

The purpose of this study is to describe the petrography, Sr, Nd, Pb and O isotopic composition, and the major and trace element geochemistry of the lavas and dykes, and to use these data to assess their petrogenesis. Particular attention is paid to the role of incorporation of subducted sediments vs crustal contamination in the evolution of these lavas [see Davidson, (1985, 1987), White & Dupré (1986) and Davidson *et al.* (1993)].

PETROGRAPHY

The majority of the lavas and dykes exposed on Bequia are plagioclase–olivine–clinopyroxene–magnetite-phyric basalts, and occur with minor clinopyroxene–orthopyroxene–plagioclase–magnetite-phyric andesites. One andesite sample (BQ20) contains amphibole phenocrysts (Table 1). The lavas and dykes typically contain between 30% and 75% phenocrysts dominated by oscillatory-zoned calcic plagioclase (~An_{60-80}). The feldspar phenocrysts commonly show a narrow spongy zone near their margins, which is indicative of partial dissolution (melt channels). The clinopyroxene phenocrysts are also prominently zoned. Intratelluric magnetite is more abundant in the andesites than in the basalts (Table 1). The groundmass comprises intergranular to intersertal, random to pilotaxitic, intergrowths of plagioclase laths, pyroxene prisms and grains, opaque mineral grains and plates, and minor glass. Sample BQ19 contains small irregular crystals of phlogopite and unaltered brown hornblende intergrown with the groundmass. Sample BQ2 also contains small irregular crystals of groundmass amphibole.

A limited amount of post-magmatic alteration has affected some of the samples. All of the olivine phenocrysts present in these lavas are partially to

Downloaded from https://academic.oup.com/petrology/article/37/1/117/1530492 by guest on 21 August 2022

Table 1: Mineralogy and petrography of the Bequia lavas and dykes

Sample no.	Rock type	% Phenocrysts ol	cpx	opx	pl	amph	mt	Matrix	Alteration
Isotopically homogeneous suite									
BQ1	basalt lava	5	5		25		1	pilotaxitic	p.i. of ol
BQMFT1	basalt lava	5	15		50			intergranular	p.i. of ol
BQ4	basalt lava		10		30			intersertal	none
BQ5	basalt lava	7	15		50		<1	intergranular	p.i. of ol
BQ8	basalt lava	8	5		30		1	pilotaxitic	c.i. of ol
BQ9	basalt lava	10	5		30			intergranular	p.i. of ol
BQ10	basalt lava	10	10		20		<1	intergranular	c.i of ol
BQ14	andesite dyke	4	1	5	25		>2	intergranular	none
BQ15	basalt lava		2		25		<1	pilotaxitic	none
BQ16	andesite dyke		5		30		1	pilotaxitic	p.i. of ol
BQ25	basalt lava	8	5		30		<1	pilotaxitic	p.i. of ol
BQ26	basalt lava		1		40			pilotaxitic	none
Isotopically diverse suite a									
BQ2	basalt lava	20	15		40		1	intergranular	p.i. of ol
BQMFT3	basalt lava	5	8		30			intergranular	none
BQ11	basalt lava	10	5		40		1	intergranular	p.i. of ol
BQ12	basalt lava	10	5		30			intergranular	c.i. of ol
BQ19	basalt lava	2	5		50			intergranular	c.i. of ol
Isotopically diverse suite b									
BQ3	basalt lava	10	15		25		<1	pilotaxitic	p.i. of ol
BQMFT4	basalt lava	8	5		40			intergranular	c.i. of ol
BQ6	basalt lava	10	10		30		1	intergranular	p.i. of ol
BQ7	basalt lava	5	5		40		<1	intersertal	p.i. of ol
BQ17	basalt lava	15	20		55		>2	intergranular	p.i. of ol
BQ18	andesite lava		1	5	40		3	felsitic	s. of pl
BQ20	andesite lava		2	5	35	2	3	intergranular	op rim on amph
Plutonic blocks									
BQMFT8	gabbro		6		80	12	2	adcumulate	
BQ13	gabbro	3			30	67		adcumulate	

Minerals: ol, olivine; cpx, clinopyroxene; opx, orthopyroxene; pl, plagioclase; amph, amphibole; mt, magnetite.
Alteration: p.i., partial iddingsitization; c.i., complete iddingsitization; s., saussuritization; op, opacite.

completely replaced by iddingsite. Orthopyroxene phenocrysts occur only in samples BQ18 and BQ20 (Table 1), and are oxidized around their margins and along fractures. The amphibole phenocrysts in BQ20 (Table 1) are partially rimmed by opacite. In BQ7 the interstitial glass is partially replaced by fine-grained aggregates of chloritic minerals.

The plutonic blocks that commonly occur in the epiclastic rocks are made up mainly of cumulus crystals of relatively unzoned plagioclase ($\sim An_{55}$), clinopyroxene and olivine, and intercumulus and cumulus greenish brown hornblende and opaques (Table 1).

Petrographically, all of the lavas appear to belong to one sequence of basalts and andesites. The phenocryst assemblages of the basalts and andesites, and the cumulate mineralogy of the plutonic blocks, are typical of those forming below the solidus from hydrous tholeiitic and andesitic magmas at pressures below $\sim$3 kbar and at temperatures between 1200°

Downloaded from https://academic.oup.com/petrology/article/37/1/117/1530492 by guest on 21 August 2022

and 900°C (Green, 1982, figs 6 and 7). This suggests that the lava sequence was formed by fractional crystallization. However, the oscillatory zoning and the presence of melt channels in the plagioclase phenocrysts, and the zoning in the clinopyroxenes, suggest that the crystallization process was complex.

ANALYTICAL METHODS

The major elements, and most of the trace elements, were determined by X-ray fluorescence techniques on fused glass discs and pressed powder pellets, respectively. Major element compositions on most samples were determined at Windsor using a PW1410 Philips X-Ray Spectrometer. The major elements contents of BQ2, -18, -19 and -26, BQMFT1, -2, -4 and -8, and all of the trace element analyses, were determined at Royal Holloway, University of London. Errors on major element determinations vary from a minimum of 0·006% (2σ) on P_2O_5 and MnO to 0·15% (2σ) SiO_2, and are given in Table 2. Matrix corrections for trace elements were calculated from major element compositions. Reproducibility is ±1 p.p.m. or 1% (2σ), whichever is worse, for most trace elements, except Nb(±0·2 p.p.m., 2σ), Pb and Th (±0·3 p.p.m., 2σ), Rb and Y (±0·4 p.p.m., 2σ) and Cl (±20 p.p.m., 2σ) (Table 2).

Sr, Nd and Pb were separated for isotopic analysis using conventional ion exchange techniques following dissolution in FEP beakers (Sr) or Savilex capsules (Nd and Pb). Some Sr and Pb samples, indicated in Table 3, were leached for 1 h in hot 6 M HCl, and rinsed several times with pure water, before dissolution. Sr and Nd were analysed using techniques reported by Thirlwall (1991*a*, 1991*b*), and are consistent with SRM 987, $^{87}Sr/^{86}Sr = 0{\cdot}710248 \pm 20$ and La Jolla $^{143}Nd/^{144}Nd$ of $0{\cdot}511857 \pm 8$ (2 SD). Comparison of determinations on the same samples shows that leaching may reduce the $^{87}Sr/^{86}Sr$ ratios by up to 0·000030 (Table 3). Pb was loaded with silica gel and H_3PO_4, on single Re filaments, and analysed in static mode on the Royal Holloway five-collector VG354 mass spectrometer. Within-run errors are better than 0·013%/amu (2 SE), and reproducibility is better than 0·4%/amu.

Rare earth elements (REE; Table 4) and uranium (Table 2) were determined by isotope dilution using the technique of Thirlwall (1982) modified for the Royal Holloway five-collector VG354 mass spectrometer. Errors on isotope dilution determinations are <1% (2 SD).

Oxygen isotope ratios (Table 3) were determined on carefully hand-picked phenocrysts of augite and olivine. Between 1 and 2 mg of mineral separate were analysed using the Royal Holloway laser fluorination system and VG Prism mass spectrometer [details have been given by Mattey & Macpherson (1993)]. Oxygen yields were, within error, 100%, and $\delta^{18}O$ was standardized to NBS30 biotite at 5·15‰. Reproducibility is around ±0·1‰ (2 SD).

ISOTOPIC DATA

Isotopic systematics are used to divide the Bequia lavas and dykes into two suites (Table 3). The first suite has a small range of Sr–Nd–Pb isotopes and relatively low $\delta^{18}O$ values, and is designated the isotopically homogeneous suite (IHS). When compared with the IHS, the second suite is characterized by large ranges and high values of Sr and Pb isotope ratios, a large range and low values of Nd isotope ratios, and relatively high $\delta^{18}O$ values. It is designated the isotopically diverse suite (IDS) (Table 3, Figs 2–4). The lavas of the two suites are interlayered and show no systematic geographic or temporal distribution (Fig. 1, Table 1).

In the IHS the $^{87}Sr/^{86}Sr$ ratios (0·70404–0·70460) are slightly higher than those of mid-ocean ridge basalt (MORB), and the $^{143}Nd/^{144}Nd$ ratios (0·51296–0·51300) are similar to those of MORB (Table 3). The Pb isotope ratios of the IHS vary over a limited range ($^{206}Pb/^{204}Pb = 19{\cdot}36$–$19{\cdot}51$) (Table 3). The tholeiitic rocks of neighbouring St Vincent are petrographically and chemically similar to the IHS basalts. Regression lines based on the Bequia data are collinear with the elongate fields defined by the St Vincent data (White & Dupré, 1986; M. F. Thirlwall, unpublished data) on Pb–Pb diagrams (Fig. 3). The data from the IHS also overlap with the St Vincent fields on Sr–Nd, Pb–Sr and Pb–Nd isotope plots (Figs 2 and 4). These factors suggest the two suites were derived from similar sources and have similar evolutionary histories.

The linear array defined by the combined IHS and St Vincent data on the $^{206}Pb/^{204}Pb$ vs $^{207}Pb/^{204}Pb$ isotope diagram is displaced upwards from, and slopes more steeply than, the MORB trend (Fig. 3). On $^{206}Pb/^{204}Pb$ vs $^{208}Pb/^{204}Pb$ diagrams the combined data lie within the MORB field but define a linear trend which is steeper than that of MORB. In addition, the linear trends of the combined Pb data extrapolate into the fields defined by sediments from DSDP Hole 543 (Fig. 3), which are considered to be representative of those currently being subducted beneath the arc (White & Dupré, 1986).

In the IDS the $^{87}Sr/^{86}Sr$ and $^{143}Nd/^{144}Nd$ ratios range from 0·70840 to 0·70776 and from 0·51273 to

Downloaded from https://academic.oup.com/petrology/article/37/1/117/1530492 by guest on 21 August 2022

Table 2: Geochemistry of lavas, dykes and cumulate blocks from Bequia

			Isotopically homogeneous suite											Plutonic blocks	
	2σ	Sample no :	BQ1	BQ1MFT	BQ4	BQ5	BQ8	BQ9	BQ10	BQ14	BQ15	BQ16	BQ25	BQ26	BQMFT8	BQ13
wt%																
SiO_2	±0·15		51·02	50·34	51·79	49 48	50·95	51·44	49 58	56·1	51·21	53·2	51·42	51·07	47·54	44·11
TiO_2	±0·008		0·91	0·753	1·036	0·727	0·86	0·952	0·787	0·753	0·844	0·939	0·85	0·915	0·721	2·382
Al_2O_3	±0·10		21·03	17·22	22·77	16·5	20·96	19·8	18·4	19·31	20·77	20·38	18·39	21·73	28·11	20·23
ΣFe_2O_3	±0·10		8·81	9·72	8·66	9·99	8·87	9·64	10·15	8·58	8 21	8·71	9·62	8·92	5·25	9·93
MnO	±0·006		0·166	0·195	0 137	0·235	0·18	0·18	0·205	0·137	0·166	0·182	0·184	0·144	0·099	0·121
MgO	±0·10		3·39	7·51	2·9	7 9	3·73	3·27	6·01	2·52	3·48	2·52	5·27	3·21	2·63	8·81
CaO	±0·06		10·16	11·55	9·79	10·98	10·81	10·29	11·05	7·78	10 35	9·42	10·48	10·57	13·53	12·3
Na_2O	±0·10		3·5	2·22	2·69	2 56	3·16	3·18	2·55	3·67	3·08	3·25	3·11	3·03	1·93	1·51
K_2O	±0·008		0·598	0·317	0·228	0·321	0·39	0·448	0·311	0·625	0·403	0·398	0·404	0·388	0·116	0·279
P_2O_5	±0·006		0·176	0·084	0·137	0·095	0·12	0·13	0·104	0·171	0·131	0·13	0·12	0·099	0·035	0·031
Total			99·76	99·91	100·14	98·79	100·03	99·33	99·15	99·65	98·64	99·13	99·85	100·08	99·96	99·70
LOI			0·61	0·17	3·13	0·46	0·39	0·17	0·82	0·55	0 2	0·55	0·12	0·81	0·38	0·97
FeO*/MgO			2·338	1·165	2·687	1·138	2·140	2·653	1·520	3·064	2·123	3·110	1·643	2·500	1·796	1·014

(continued on next page)

Downloaded from https://academic.oup.com/petrology/article/37/1/117/1530492 by guest on 21 August 2022

Table 2: continued

		Isotopically homogeneous suite											Plutonic blocks	
	2σ	Sample no : BQ1	BQ1MFT	BQ4	BQ5	BQ8	BQ9	BQ10	BQ14	BQ15	BQ16	BQ25	BQ26	BQMFT8	BQ13
p.p.m.															
Ni	±1	23	64	13	67	18	18	43	16	28	17	36	nd	16	29
Cr	±3	26	135	19	148	42	38	100	31	57	32	90	nd	4	80
V	±2	281	270	314	270	249	282	247	160	242	269	267	nd	66	409
Sc	±1	24	40	42	41	31	30	36	21	27	30	35	nd	11	64
Cu	±1	74	54	120	70	138	115	65	72	51	143	49	nd	10	37
Zn	±1	70	75	77	73	73	77	80	90	72	79	75	nd	39	59
Cl	±20	31	879	726	315	nd	74	335	22	21	87	255	nd	318	303
Ga	±1	20	16	18	15	18	20	18	19	20	20	18	nd	22	19
Pb	±0·3	1·1	2·2	1·9	0·9	1·8	2·1	2·8	2·4	1·6	1·9	1·5	nd	1 9	0·1
Sr	±1	394	204	212	200	213	231	240	229	302	253	215	nd	461	291
Rb	±0·4	8·4	5·8	1·4	6·4	7·6	8·8	5	12·3	6·7	4·7	7·3	nd	1·5	2·2
Ba	±2	124	100	55	94	85	112	77	134	91	103	84	nd	63	162
Zr	±0·8	76	47	62	48	62	67	49	95	64	76	58	nd	20	42
Nb	±0·2	6·1	1·6	2·4	1·4	1·7	2·5	2	3·3	3·8	2·6	2·5	nd	1 6	5
U	±0·01	0·913	nd	nd	0·356	nd	nd	nd	0·775	nd	nd	nd	0·393	nd	nd
Th	±0·3	1·6	0·8	1·1	0·8	1·2	1·5	1	2·1	1	1·2	0·8	nd	0·6	0
Y	±0·5	23 4	26·9	29·8	21	21·6	24·4	21·2	33·8	23·7	27·9	20·5	nd	5·4	33
La	±1·5	7·8	5·9	4·3	3·8	2·9	5·3	4·8	7·3	4·6	5·1	nd	nd	3·5	1·5
Ce	±1·5	17·2	13·4	12·4	8·5	12·1	13·8	10·1	16·8	12·3	12·4	8·8	nd	7·6	10·48
Nd	±1·0	11·3	10	9·5	6·7	8·5	9·2	9·4	12	9·8	9·6	6·4	nd	4·1	12·8
Elemental ratios															
Ti/V		19 41	16·72	19·78	16·14	20·71	20·24	19·10	28·21	20·91	20·93	19·09	nd	66·50	34·91
Zr/Nb		12·46	29·38	25·83	34·29	36·47	26·80	24·50	28·79	16·84	29·23	23·20	nd	12·50	8·40
Zr/Y		3·25	1·75	2·08	2·29	2·87	2·75	2·31	2·81	2·70	2·72	2·83	nd	3·70	1·27
K/Rb		591·02	453·75	1352·04	416·40	426·02	422·65	516·38	421·85	499·36	703·02	459·45	nd	642·02	1052·84
Rb/Ba		0·068	0·058	0·025	0·068	0·089	0·079	0·065	0·092	0·074	0·046	0·087	nd	0·024	0·01
Ba/La		15·90	16·95	12·79	24·74	29·31	21·13	26·55	18·36	19·78	20·20	nd	nd	18·00	108·00
Pb/Ce		0·064	0·164	0·161	0·106	0·149	0·152	0·241	0·143	0·130	0·153	0·170	nd	0·250	0 010

Downloaded from https://academic.oup.com/petrology/article/37/1/117/1530492 by guest on 21 August 2022

		Isotopically diverse suite a					Isotopically diverse suite b						
	2σ Sample no.:	BQ2	BQ3MFT	BQ11	BQ12	BQ19	BQ3	BQMFT4	BQ6	BQ7	BQ17	BQ18	BQ20
wt%													
SiO_2	±0·15	49·49	50·36	50·39	50·27	50·28	53·07	49·73	49 87	51·47	50·82	61·02	59·22
TiO_2	±0·008	0·804	0·839	0·828	0·832	0·904	0·85	0·914	1·082	0·92	1·041	0·525	0·543
Al_2O_3	±0·10	18·42	19·55	19·08	18·9	22·18	19·27	21·33	19·39	20·48	18·98	18·24	17·78
ΣFe_2O_3	±0·10	9·42	9·12	9·22	9·2	8·64	8·81	9·14	9·77	10·2	9·88	7·47	8·02
MnO	±0·006	0·178	0·171	0·172	0·16	0·176	0·174	0·144	0·194	0·18	0·222	0·1	0·163
MgO	±0·10	7·1	5·79	5·94	5·34	3·03	3·36	4·14	4·68	3·46	4·51	1·93	2·32
CaO	±0·06	11·71	11·22	10·62	11·25	10·39	9·22	11·52	10·18	10·02	10·46	5·57	6·27
Na_2O	±0·10	2·52	2·52	2·7	2·4	3 29	3·36	2·84	3·31	2·89	3·12	3·93	3·69
K_2O	±0·008	0·584	0·581	0·567	0·526	1·119	0·662	0·281	0·571	0·27	0·542	0·926	0·788
P_2O_5	±0·006	0·105	0·099	0·107	0·104	0·171	0·128	0·089	0·115	0·14	0·12	0·173	0·174
Total		100·33	100·25	99·62	98·98	100·18	98·90	100·13	99·16	100·03	99·70	99·88	98·97
LOI		0·16	−0·08	0·17	0·41	0·43	0·28	0·52	0·28	0·98	0·3	1·29	1·28
FeO*/MgO		1·194	1·417	1·397	1·550	2·566	2·359	1·987	1·878	2·653	1·971	3·483	3·111

(continued on next page)

Downloaded from https://academic.oup.com/petrology/article/37/1/117/1530492 by guest on 21 August 2022

Table 2: continued

			Isotopically diverse suite a					Isotopically diverse suite b						
	2σ	Sample no.:	BQ2	BQ3MFT	BQ11	BQ12	BQ19	BQ3	BQMFT4	BQ6	BQ7	BQ17	BQ18	BQ20
p.p.m.														
Ni	±1		37	22	26	25	11	17	20	14	10	15	8	10
Cr	±3		126	47	75	90	34	49	47	38	19	39	26	33
V	±2		151	181	183	154	56	190	247	184	163	235	49	50
Sc	±1		27	29	32	32	15	27	32	28	22	32	11	11
Cu	±1		45	99	41	43	37	51	45	29	26	28	23	22
Zn	±1		85	80	79	83	113	79	77	79	86	84	92	85
Cl	±20		46	158	62	194	121	92	1145	224	nd	36	20	84
Ga	±1		18	18	18	19	23	20	19	19	20	19	21	21
Pb	±0·3		4·2	3	3·3	4·8	20·8	3 3	3·5	2·2	3·1	1·9	5·9	6·0
Sr	±1		271	276	265	267	411	257	259	264	298	247	292	305
Rb	±0·4		18·3	19·1	18	16·7	43·2	20·2	2·5	15·2	6	15	36·9	30
Ba	±2		136	143	136	237	254	154	135	124	101	110	226	219
Zr	±0·8		75	72	73	73	139	83	65	76	77	73	132	128
Nb	±0·2		4·0	4·3	4·0	4·3	10·1	3·6	2·6	3·4	3·5	3	5·1	5·3
U	±0 01		1·353	nd	1·068	nd	nd	nd	nd	nd	0·386	nd	nd	0·386
Th	±0·3		3	3·2	3·2	2·5	8·2	3·5	2·4	2	1·9	2	5·2	5·9
Y	±0·5		22·7	23·6	23	32·5	31·7	26·1	25·8	26·3	23·8	23·8	24·1	23·2
La	±1·5		9·5	11·1	9·1	9·6	24·2	8·4	8·9	6·5	6·3	5·9	16·1	14
Ce	±1·5		20·6	22·6	18·8	17·4	46·7	16 9	13·6	15	14·1	15·9	29·8	31
Nd	±1·0		11·4	12·3	10·7	11·7	22·1	11·4	11·7	9·74	10·1	9·9	17·5	14·6
Elemental ratios														
Ti/V			31·92	27·79	27·12	32·39	96·78	26 82	22 18	35 25	33·84	26·56	64·23	65·11
Zr/Nb			18·75	16·74	18·25	16·98	13·76	23·06	25·00	22·35	22·00	24·33	25·88	nd
Zr/Y			3·30	3·05	3·17	2·25	4·38	3·18	2·52	2·89	3·24	3·07	5·48	4·77
K/Rb			264·94	252·54	261·51	261·49	215·04	272·08	933·14	311·87	373·59	299·98	208·34	218·07
Rb/Ba			0·135	0·134	0·132	0·070	0·170	0·131	0·019	0·123	0·059	0·136	0·163	0·137
Ba/La			14·32	12·88	14·95	24·69	10·50	18·33	15·17	19·08	16·03	18·64	14·04	nd
Pb/Ce			0·204	0·133	0·176	0·276	0·445	0·195	0·257	0·147	0·220	0·119	0·198	nd

LOI, loss on ignition; nd, not determined.

Downloaded from https://academic.oup.com/petrology/article/37/1/117/1530492 by guest on 21 August 2022

Table 3: Isotopic compositions of selected samples of the Bequia lavas and dykes

Sample no.	$^{87}Sr/^{86}Sr$	ε_{Sr}	$^{143}Nd/^{144}Nd$	ε_{Nd}	$^{206}Pb/^{204}Pb$	$^{207}Pb/^{204}Pb$	$^{208}Pb/^{204}Pb$	$\delta^{18}O$ cpx	$\delta^{18}O$ ol	$\delta^{18}O$ corr cpx*
Isotopically homogeneous suite										
BQ1	0·70460±1	1 2	0·512995±7	7 0	19·386†	15·709	38·824	5·44		5·64
BQ1	0·70458±1†	1·1								
BQ1MFT	0·70437±1	−1·9								
BQ4	0·70421±2†	−4·1								
BQ5	0·70434±1†	−2·3	0·512982±12	6 7	19·511	15·742	39·010	5·53	5·21	5·73
BQ8	0·70438±1†	−1·7						5·35		5·55
BQ9	0·70438±1	−1·8						5·64		5·84
BQ10	0·70438±1†	−1·7								
BQ14	0·70447±1	−0·4								
BQ14	0·70437±1†	−1·9	0·512960±8	6·3	19·398	15·734	38·911			
BQ15	0·70408±1	−6·0								
BQ16	0·70429±1	−3·0								
BQ25	0·70404±1†	−6·5			19 36†	15·723	38·893	5·56		5·76
BQ25	0·70410±1	−5·7	0·512965±5	6·4						
BQ26	0·70425±1	−3·5	0·512995±8	7·0	19·480	15·758	39·070			
Isotopically diverse suite a										
BQ2	0·70623±1	24·5	0·512540±4	−1·9	20·032	15·831	39·509	6·58	5·82	6·78
BQ3MFT	0·70654±1	28·9								
BQ11	0·70655±1†	29·0	0·512466±3	−3·4	20·004	15·820	39·496			
BQ12	0·70652±2†	28·6	0·512473±4	−3·2	19·985†	15·817	39·485			
BQ19	0·70766±1	44·7	0·512257±3	−7·4	20·157	15·851	39·654	7·62‡		7·82
Isotopically diverse suite b										
BQ3	0 70502±1	7·3	0·512803±7	3 2				5 98		6·18
BQ3	0·70499±1†	6·8								
BQMFT4	0·70484±3	4·9	0·512780±6	2·8						
BQMFT4	0·70484±1†	4·8								
BQ6	0·70540±1	12·7	0·512726±3	1 7	19·749	15·773	39·218	6·28	6·12	6 48
BQ7	0·70501±1	7·3	0·512806±4	3 3	19·768	15·779	39·254			
BQ17	0·70506±1†	7·9								
BQ18	0·70518±1	9 4	0·512754±3	2·3						
BQ20	0·70519±1	9·8	0·512750±6	2·2						

*Measured values corrected using the equations of Kalamarides (1986).
†Isotopic ratios determined on leached samples.
‡Mean of two determinations.

Downloaded from https://academic.oup.com/petrology/article/37/1/117/1530492 by guest on 21 August 2022

Table 4: Isotope dilution rare earth element contents (p.p.m.) and ratios of selected samples of Bequia lavas and dykes

	Isotopically homogeneous suite				
	BQ1	BQ5	BQ14	BQ25	BQ26
La	7·77	3·83	7·3		4·832
Ce	17·22	8·48	16·83	8·78	10·02
Nd	11·25	6·720	12·04	6·417	9·004
Sm	2·948	2·017	3·371	1·893	2·729
Eu	1·002	0·738	1·109	0·695	0·998
Gd	3·27	2·66	4·26	2·52	3·48
Dy	3·66	3·24	4·68	3·26	3·68
Er	2·285	2·04	3·18	2·052	2·312
Yb	2·237	1·989	3·22	1·999	2·21
Lu		0·300			

	Isotopically diverse suite a				Isotopically diverse suite b		
	BQ2	BQ11	BQ12	BQ19	BQ6	BQ7	BQ18
La	9·53	9·06	9·56	24·21	6·51	6·31	16·14
Ce	20·63	18·80	17·4	46·67	15·01	14·14	29·79
Nd	11·40	10·650	11·67	22·09	9·741	10·08	17·46
Sm	2·876	2·664	3·001	4·677	2·722	2·763	3·729
Eu	0·903	0·830	0·922	1·286	0·917	0·964	1·040
Gd	3·37	3·02	3·84	4·81	3·28	3·20	3·88
Dy	3·60	3·65	4·40	4·74	4·15	3·829	3·72
Er	2 291	2·312	2·87	3·05	2·59	2·353	2·316
Yb	2·21	2·253	2·61	3·05	2 49	2·264	2·436
Lu				0·444		0·3369	0·376

0·51226, respectively, and define a near-linear trend which extrapolates to intersect the IHS field at $^{87}Sr/^{86}Sr$ ~0·7040 and $^{143}Nd/^{144}Nd$ ~0·51295. A similarly wide range of ratios is observed on the islands of Martinique (Davidson, 1983, 1986) and St Lucia (Davidson, 1985, 1987; White & Dupré, 1986) but is not found on the large islands to the immediate north (St Vincent) or south (Grenada) of Bequia (Thirlwall & Graham, 1984; White & Dupré, 1986; M. F. Thirlwall, unpublished data). The Pb is more radiogenic in the IDS ($^{206}Pb/^{204}Pb = 19·75–20·16$) than it is in the IHS; BQ19 has the most radiogenic Pb yet reported from the Lesser Antilles ($^{206}Pb/^{204}Pb = 20·16$) (Table 3). On the Pb–Pb diagrams all IDS samples fall on linear arrays which extrapolate to cut the IHS fields at $^{206}Pb/^{204}Pb$ ~19·4 (Fig. 3). The linear trends defined on the $^{206}Pb/^{204}Pb$ vs $^{207}Pb/^{204}Pb$ diagram for the IDS are discrete from, and slope more gently than, those of the combined St Vincent–IHS field. On the $^{206}Pb/^{204}Pb$ vs $^{208}Pb/^{204}Pb$ diagram the IDS data lie very largely outside the DSDP sediment field (Fig. 3).

The measured $\delta^{18}O$‰ SMOW values of the olivine and clinopyroxene phenocrysts from the Bequia lavas vary from +5·21 to +5·64 in the IHS, and from +5·82 to +7·62 in the IDS (Table 3). Kalamarides' (1986) equations show that the differences between the $\delta^{18}O$ values for olivine and clinopyroxene crystallizing from a basaltic melt should be ~0·4, but in the Bequia samples the differences range from 0·16 to 0·76 (Table 3). The clinopyroxenes show no sign of alteration but many of the olivines show partial or complete iddingsitization in thin section. This large range of differences between the olivine and clinopyroxene values suggests that the apparently fresh olivine crystals, hand picked for analysis, had been subjected to incipient alteration which also affected their $\delta^{18}O$ values. The oxygen data derived from the olivines are therefore not

Downloaded from https://academic.oup.com/petrology/article/37/1/117/1530492 by guest on 21 August 2022

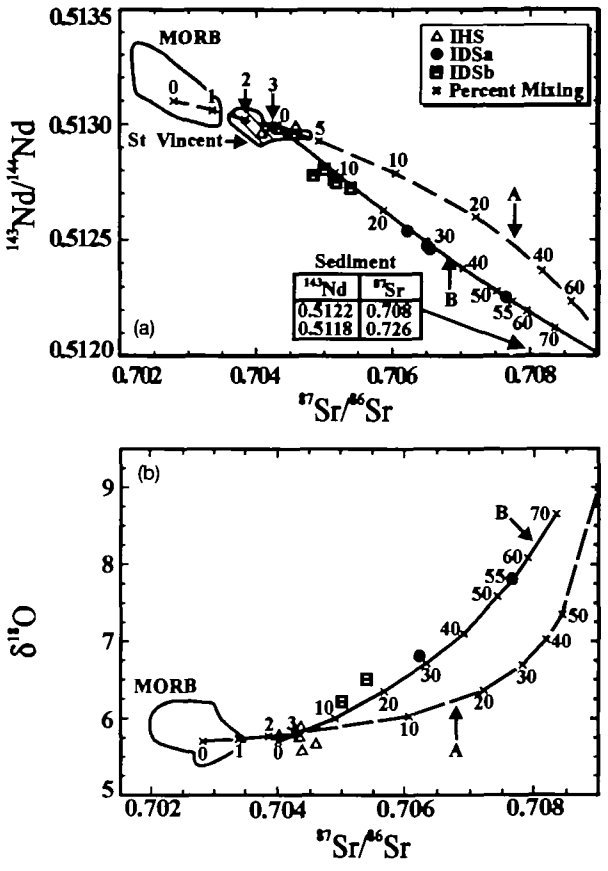

Fig. 2. Plots of $^{87}Sr/^{86}Sr$ vs $^{143}Nd/^{144}Nd$ ratios (a) and $\delta^{18}O$ values (b) in representative samples of the Bequia lavas and dykes. Also shown are St Vincent fields (M. F. Thirlwall, unpublished data), and the MORB fields and DSDP Hole 543 sediment data from White & Dupré (1986), together with mixing curves defined by the preferred models of the petrogenesis of the IHS and IDS lavas. Curve A, IHS; Curve B, IDS; crosses on mixing curves and adjacent numbers show percentages of subduction component (Curve A) and crustal component (Curve B), respectively (see Tables 6 and 7 for details).

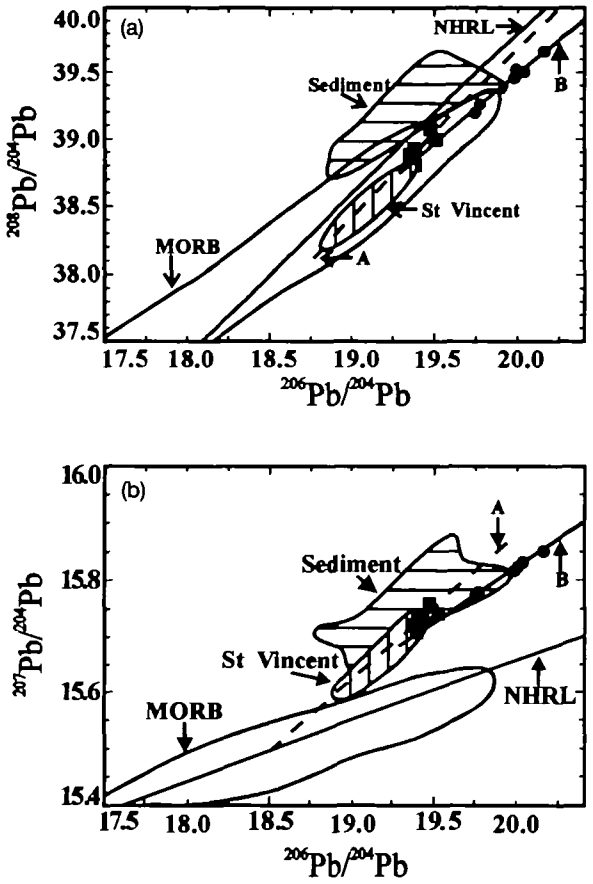

Fig. 3. Plots of $^{206}Pb/^{204}Pb$ vs $^{208}Pb/^{204}Pb$ (a) and $^{207}Pb/^{204}Pb$ ratios (b) of representative samples of the Bequia lavas and dykes. Also shown are the MORB and St Vincent fields, and DSDP Hole 543 sediment data (sources as above). Northern Hemisphere Reference line (NHRL; Hart, 1984), and regression lines through IHS (Curve A) and IDS (Curve B) data points. Symbols as in Fig. 2.

plotted (Fig. 2) or used in petrogenetic modelling. The plots and models (Fig. 2) use the fresh clinopyroxene $\delta^{18}O$ values corrected for melt–clinopyroxene fractionation (cpx-corr, Table 3) by a factor of +0·20 (Kalaramides, 1986).

The linear trends defined by the combined Pb isotope data from the Bequia IHS and St Vincent suites (Fig. 3) are indicative of binary mixing in their petrogenesis. These trends extrapolate to intersect the fields defined by MORB and the locally subducting sediments. This implies that the Pb isotope ratios of the IHS may be explained in terms of mixing of a depleted mantle (MORB) component and a subduction component at least partly derived from the sediments. The $^{87}Sr/^{86}Sr$ and $^{143}Nd/^{144}Nd$ distributions in the IHS and St Vincent suite are also compatible with this conclusion (Figs 2 and 4).

The Lesser Antillean mantle source is estimated to have an oxygen isotope composition $\delta^{18}O = +5{\cdot}7 \pm 0{\cdot}3$ whereas crustal materials are characterized by higher values, generally in excess of $\delta^{18}O \sim +10$ (Davidson & Harmon, 1989). James (1981) suggested that it may be possible to distinguish between crustal and mantle contamination using $^{18}O/^{16}O$ ratios but others maintain that it is not (Vroon *et al.*, 1993). None the less, the Bequia lava $\delta^{18}O$ values do fall into two separate groups. The relatively low $\delta^{18}O$ values ($<5{\cdot}7$) of the fresh hand-picked clinopyroxenes from the IHS are virtually indistinguishable from those determined on clinopyroxenes from 70 varied mantle peridotites [Mattey *et al.* (1994); see also James (1981) and Kyser (1990)]. We suggest that this indicates that

Downloaded from https://academic.oup.com/petrology/article/37/1/117/1530492 by guest on 21 August 2022

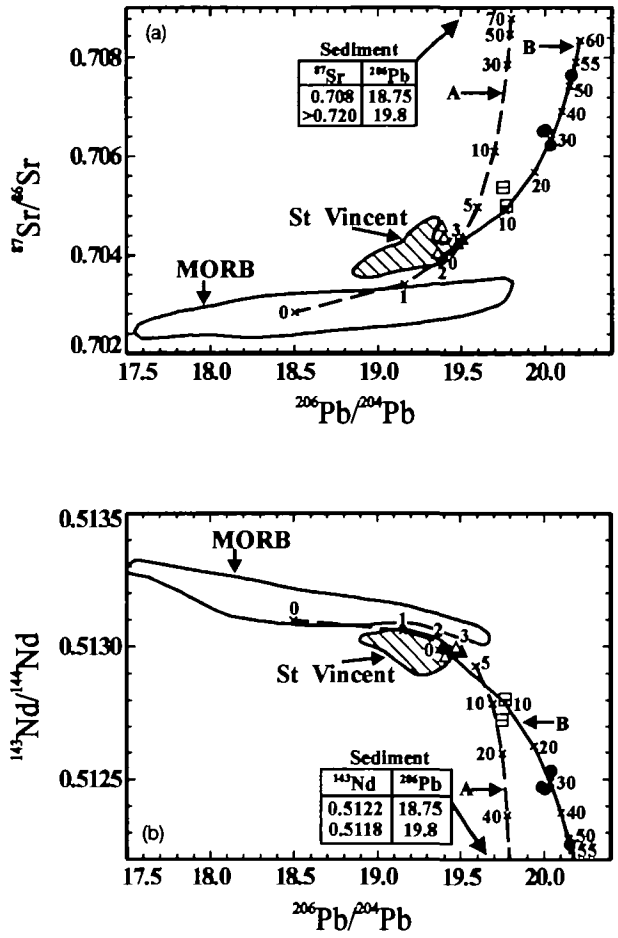

Fig. 4. Plots of $^{206}Pb/^{204}Pb$ vs $^{87}Sr/^{86}Sr$ (a) and $^{143}Nd/^{144}Nd$ ratios (b) of representative samples of the Bequia lavas and dykes. Also shown are the MORB and St Vincent fields and sediment data (sources as above) and the mixing curves defined by the preferred mixing models for the petrogenesis of IHS (Curve A) and IDS (Curve B) (see Tables 6 and 7 for details). Symbols as in Fig. 2.

the IHS melts were formed by mantle-dominated processes.

The distributions Pb isotope ratios and the near-linear distributions of the $^{87}Sr/^{86}Sr$ vs $^{143}Nd/^{144}Nd$ ratios of the IDS lavas are strongly suggestive of binary mixing. The extrapolation of these trends to intersect the fields defined by the combined St Vincent and IHS data (Figs 2–4) strongly implies that melts isotopically similar to the IHS melts were involved in the mixing. The trend of $^{206}Pb/^{204}Pb$ vs $^{207}Pb/^{204}Pb$ of the IDS cannot be explained in terms of subducted sediment mixing with a depleted MORB reservoir or any other recognized mantle reservoir (Hart, 1984) because it does not intersect the sediment field (Fig. 3). The high Pb isotope ratios, and the very high $\delta^{18}O$ values (up to +7·62), which are typical of the IDS, suggest that a crustal component was important in its petrogenesis (James, 1981; Kyser, 1990; Thirlwall *et al.*, 1995). Similar trends recognized in lavas in Martinique are interpreted as resulting from mixing of Mesozoic arc crust, as represented by the Gros Islet garnet-bearing dacite ($^{206}Pb/^{204}Pb = 19·915$), with melts derived from a subduction-modified depleted mantle (Davidson & Harmon, 1989). However, the most extreme isotopic composition on Bequia (BQ19 $^{206}Pb/^{204}Pb = 20·157$) implies that the crustal component must have an even higher radiogenic Pb ratio. Such a high $^{206}Pb/^{204}Pb$ ratio is consistent with a Precambrian origin for the crustal component. The $\delta^{18}O$ values covary systematically with the radiogenic isotope ratios (Table 3, Fig, 2) and are interpreted as resulting from progessively increasing amounts of assimilation of crustal material by the IHS melts. Detailed models of the genesis of the two suites, which utilize chemical as well as isotopic constraints, are discussed below.

GEOCHEMISTRY AND PETROGENESIS

The chemical compositions of the lavas confirm their subdivision, using isotopic data, into the IHS and the IDS, and may also be utilized with the isotopic data to further sub-divide the IDS. Plots of MgO (and SiO_2) vs $^{87}Sr/^{86}Sr$ and $^{143}Nd/^{144}Nd$ define the IDSa, in which there is a systematic increase in $^{87}Sr/^{86}Sr$, and a systematic decrease in $^{143}Nd/^{144}Nd$, with decreasing MgO (and increasing SiO_2) contents (Fig. 5). The isotopic ratios of the IDSb samples differ from those of the IDSa in being relatively constant over the full range of MgO (and SiO_2) contents in the suite. They are also systematically higher (Sr, Pb, O), or lower (Nd), than those of the IHS (Table 3, Fig. 5).

In spite of the isotopic differences among the suites, the petrographic data cited above suggest that the St Vincent tholeiites and all of the Bequia lavas formed by relatively low-pressure fractional crystallization of hydrous magmas. This conclusion is supported by the observations that all of the IHS and IDS lavas have high alumina ($Al_2O_3 > 16·7$ wt %), and low MgO (<8·0 wt %), Ni (<67 p.p.m) and Cr (<148 p.p.m.) contents (Table 2), and could not have been in equilibrium with the mantle. The nearly constant isotopic ratios over the complete range of MgO (and SiO_2) contents in the IHS suggest that the fractional crystallization may have occurred in a closed system. However, it is also possible that open system assimilation–fractional crystallization (AFC), in which the magma and assimilant had similar isotopic characteristics, occurred (Hildreth & Moorbath, 1988). The sys-

Downloaded from https://academic.oup.com/petrology/article/37/1/117/1530492 by guest on 21 August 2022

Table 5: Major element fractionation models for Bequia lavas and dykes

	ol %	cpx %	pl %	mt %	amph %	Σr^2	*F*
Isotopically homogeneous suite							
BQ5 to BQ25	4·8 (Fo_{86})	11·8	3·0	0·6		0·03	0·80
BQ25 to BQ8	1·1 (Fo_{81})	7·2	−11·2 (An_{92})	0·5		0·06	1·03
BQ8 to BQ14	2·6	13·5	42 (An_{74})	4·4		0·07	0·38
Isotopically diverse suite a							
BQ2 to BQ12	3·2 (Fo_{85})	6·9	6·7 (An_{92})	0·7		0·17	0 82
BQ12 to BQ19	2·2 (Fo_{81})	13·4	−5·8 (An_{92})	−0·8		0·82	0 91
Isotopically diverse suite b							
BQ6 to BQ3	3 9 (Fo_{79})	8·9	25·0 (An_{74})	3·8		0·16	0·58
BQ3 to BQ18		4·8	31·0 (An_{74})	3·3	14·8	0·08	0·46

Equilibrium olivine calculated by method of Ford *et al.* (1983). Plagioclase, magnetite and amphibole compositions taken from measurements of those in Union Island basalts and andesites (M. F. Thirlwall, unpublished data). Clinopyroxene composition taken from BQ5. Negative values are indicative of accumulation. Σr^2, sum of the squares of the residuals; *F*, fraction of melt remaining after crystallization.

The table shows the mixtures of minerals extracted, the fraction of melt left at each stage (*F*), and the fit of the model to the within-suite chemical variation (Σr^2). The chemical evolution of the IHS lavas was modelled in three stages: the first stage from the least evolved basalt in the suite (BQ5) to a basalt having intermediate composition (BQ25), the second stage from BQ25 to one of the most evolved basalts (BQ8), and the third stage from BQ8 to the only andesite analysed (BQ14). All three stages have low sums of the squares of the residuals ($\Sigma r^2 = 0{\cdot}03$ for the first stage, $\Sigma r^2 = 0{\cdot}06$ for the second stage, $\Sigma r^2 = 0{\cdot}07$ for the third stage) and fit the chemical data well. However, the proportions of the minerals extracted in modelling do not match the phenocryst assemblages present in the samples, and plagioclase accumulation is necessary in the second stage of the modelling. Thus a simple fractional crystallization model is not able to explain the IHS within-suite chemical variation. Two stages are necessary to model the chemical evolution of the IDSa—the first stage is from the least evolved basalt BQ2 to an intermediate basalt BQ12, and the second stage from BQ12 to the most evolved basalt in the suite BQ19. Both stages have high sums of squares of the residuals, $\Sigma r^2 = 0{\cdot}17$ and $\Sigma r^2 = 0{\cdot}80$, respectively, and do not fit the data well. The chemical evolution of the IDSb was modelled in two stages—from the least evolved basalt (BQ6) to an intermediate basalt (BQ3), and from BQ3 to BQ18, one of the andesites in the suite. In the first stage the model does not fit the data well ($\Sigma r^2 = 0{\cdot}34$), but in the second stage it does ($\Sigma r^2 = 0{\cdot}08$). We conclude that, as indicated by the isotopic data, simple fractional crystallization is inadequate to account for the IDS within-suite variation.

tematic increases in $^{87}Sr/^{86}Sr$, and decreases in $^{143}Nd/^{144}Nd$, with decreasing MgO and (slowly increasing SiO_2) in the IDS, strongly suggest that the suite evolved by open system fractional crystallization (AFC) involving melts isotopically similar to the IHS and a crustal component. These observations suggest that depleted mantle melts, modified by a subduction component, evolve into the IHS and IDS in shallow crustal magma chambers. The IHS results where there is essentially no crustal contribution, and the IDSa is formed where the melts interact with progressively increasing amount of crustal material. The isotopic ratios of the IDSb lavas suggest that they have a petrogenetic history intermediate between that of the IHS and the IDSa. These lavas undergo a limited amount of interaction between the melts and crustal material, causing the Sr and Pb isotope ratios and the $\delta^{18}O$ values to increase, and the Nd isotope ratios to decrease, and then further evolution of the suite takes place at constant isotopic values. This suggests that the process of crustal interaction with the subduction-modified mantle melts should be regarded as a continuum. Batches of magma undergo various amounts of AFC, causing proportional increases in their Sr and Pb isotopic ratios and $\delta^{18}O$ values, and decreases in their $^{143}Nd/^{144}Nd$. The magmas are then either cut off from the crustal assimilant or cease assimilating, and continue their evolution at constant isotopic ratios.

The tholeiitic suite of St Vincent contains picritic lavas with compositions (>12% MgO, >300 p.p.m. Ni and >800 p.p.m. Cr; M. F. Thirlwall, unpublished data) which lie outside the pyrolite liquidus field, for pressures between 1 atm and 30 kbar (Hanson & Langmuir, 1978, figs 4 and 5). We have recently partially analysed a lava from Bequia containing ~11·0% MgO. Thus the parental magmas of the St Vincent tholeiites, and of the IHS which were isotopically and petrographically similar, probably contained >12% MgO. The trends defined by the IHS and the IDSa on the isotope

Downloaded from https://academic.oup.com/petrology/article/37/1/117/1530492 by guest on 21 August 2022

Table 6: Depleted mantle-subduction component mixing model for the IHS lavas

	Source*	Sediment 1*	Sediment 2*	Sediment 3*
Sr (p.p.m.)	11	180	80	800
Nd (p.p.m.)	0·5	43	40	25
Pb (p.p.m.)	0 05	24	24	18
$^{87}Sr/^{86}Sr$	0·7028	0·7170	0·7157	0·7095
$^{143}Nd/^{144}Nd$	0·51310	0·51205	0·51200	0·51215
$^{206}Pb/^{204}Pb$	18·5	19·8	19·4†	19·0†
$\delta^{18}O$	5·7	—	—	—
Results				
SC‡:mantle Sr		5:1	10:1	20:1
	Sr	~%	~%	~%
	0·7170	2·0	1·0	1·0
	0·7157	2·5	1·5	1·0
	0·7095	5·8	3·0	2·0
SC:mantle Nd		5:1	10:1	20:1
	Nd	~%	~%	~%
	0·51205	2·0	1·0	1·0
	0·51200	2·0	1·0	1·0
	0·51215	2·5	1·0	1·0
	0·5125	4·0	1·0	1·0
SC:mantle Pb			66:1	100:1
	Pb		~%	~%
	19·8		2·5	2·0

The table above shows the percentages of the two end-members, with various isotope ratios and concentration ratios, required to match the isotopic and trace element compositions of IHS lavas. For example, the addition of 3% SC, having $^{87}Sr/^{86}Sr$ 0·7095 and SC:mantle Sr ratio of 10:1 will produce an appropriate melt. The results show that the lavas could have been produced from a depleted mantle source modified by 1–4% subduction fluid containing 50–200 p.p.m. Sr, 2·5–10 p.p.m. Nd and 3·3–5·0 p.p.m. Pb. The modified source produced may have 14–15 p.p.m. Sr, 0·6–0·8 p.p.m. Nd and 0·14–0·17 p.p.m. Pb. A preferred model (Curve A, Figs 2 and 4), which is consistent with the isotopic ratios and trace element ratios and concentrations of the IHS, has been developed using these calculations together with additional constraints described in the text as guides to the isotopic ratios and elemental concentrations of the two mixing components.

	SC	Modified mantle (mantle + 3% SC)	Model melt§	IHS lavas
Sr (p.p.m.)	110	14	~200	200–300
Nd (p.p.m.)	2	0·55	~8	6–12
Pb (p.p.m.)	4	0·17	~2·4	1–3
O (wt%)	~50	~50	~50	~50
$^{87}Sr/^{86}Sr$	0 7090	0·70426	0·70426	0·7040–0·7046
$^{143}Nd/^{144}Nd$	0 51210	0·51299	0·51299	0·51296–0·51300
$^{206}Pb/^{204}Pb$	19·8	19·4	19·4	19·4–19·5
$\delta^{18}O$	10	~5·8	~5·8	~5·55–5·84

*Data from White & Dupré (1986) except mantle Nd content (Davidson, 1986).
†These $^{206}Pb/^{204}Pb$ values are too low to provide a suitable mixing component.
‡Subduction component—SC.
§The model melt is based on the addition of 3% of the subduction component to the mantle source, followed by 10% partial melting of modified mantle and 30% fractional crystallization assuming Sr, Nd and Pb are incompatible with the mantle minerals and crystallizing minerals.

Downloaded from https://academic.oup.com/petrology/article/37/1/117/1530492 by guest on 21 August 2022

Table 7: Melt–crust assimilation fractional crystallization model for IDS lavas

	Parental melt*	Crustal assimilant	Post-Archaean shales	Model melt
Sr (p.p.m.)	150	490	48–450	410
Nd (p.p.m.)	7	23	24–48	20·8
Pb (p.p.m.)	2	35	6–43	17·4
$^{87}Sr/^{88}Sr$	0·704	0·713	<0·720	0·7077
$^{143}Nd/^{144}Nd$	0·51298	0·5112	<0·5115	0·51224
$^{206}Pb/^{204}Pb$	19·4	20·4	20·5	20·17
$\delta^{18}O$	5·7	15		7·8
	IDS lava-composition			
	BQ6	BQ2	BQ19	ΔBQ19–model melt
Sr (p.p.m.)	264	271	411	1
Nd (p.p.m.)	9·8	11·4	22·1	1·3
Pb (p.p.m.)	2·2	4·2	20·8	3·4
$^{87}Sr/^{88}Sr$	0·7054	0·7062	0·7077	0
$^{143}Nd/^{144}Nd$	0·512714	0·512540	0·51226	0·00002
$^{206}Pb/^{204}Pb$	19·75	20·03	20·16	0·01
$\delta^{18}O$	6·5	6·8	7·8	0
	IDSb	IDSa	IDSa	
% AFC	~15	~30	~55	

*The parental melt is based on the composition of St Vincent picrites. Trace element and isotopic variations were calculated using equation (15a) of DePaolo (1981*a*). In the model, *r* (ratio of the mass of the assimilant to the mass crystallized) = 0·25, D_{Sr} = 0·3, D_{Nd} and D_{Pb} = 0·1. The variations in $\delta^{18}O$ values were calculated using the method of Taylor (1980, fig. 2). The model melt is very similar in composition to BQ19 at 55% AFC (see ΔBQ19–model melt) and the fit for smaller amounts of AFC is also good (see Figs 2, 4 and 11). The IDSb samples lie off the curves plotted in Fig. 11 because of their continued crystallization when there is no isotopic evidence for further AFC.

ratio vs MgO diagrams (Fig. 5) can be extrapolated to intersect at ~12% MgO, $^{87}Sr/^{86}Sr$ ~0·704 and $^{143}Nd/^{144}Nd$ ~0·5130. These intercepts are similar to those which are defined on the isotopic diagrams (Fig. 2) and provide further support for the suggestion that the IHS and IDS evolved from similar (highly magnesian) subduction-modified mantle melts which interacted to a greater or lesser degree with crustal material. The major and trace element chemistry of the IHS and IDS is described below and is also consistent with these conclusions.

Major and trace element chemistry

The distribution of K_2O, Rb and Ba in the lavas is somewhat irregular and may imply that some of the rocks have undergone chemical as well as mineralogical alteration (Table 2). For example, BQ4 (IHS) and BQMFT4 (IDS), both of which have glassy matrices, have the highest K/Rb ratios and low K_2O, Rb and Ba contents. BQ16 (IHS) and BQ7 (IDS) also have atypically high K/Rb ratios and low Rb contents (Table 2). The four samples plot in a field below the trends defined by the remaining samples on the MgO vs K_2O diagram (Fig. 6, Table 2). K, Rb and Ba are commonly considered to be relatively mobile elements and their original concentrations may have been changed in these four samples during alteration. The samples are excluded from further discussion of these elements.

Sample BQ1 is assigned to the IHS on the basis of its isotopic ratios. Its major element chemistry and the majority of its trace element contents are consistent with this assignment (Figs 6 and 7). It also shows the same general patterns of enrichment and depletion of the incompatible elements, relative to chondrite, as the remaining samples in the suite (Fig. 8). However, it has unusually high La, U, K, P and Sr contents (Table 2). In addition, it has an

Downloaded from https://academic.oup.com/petrology/article/37/1/117/1530492 by guest on 21 August 2022

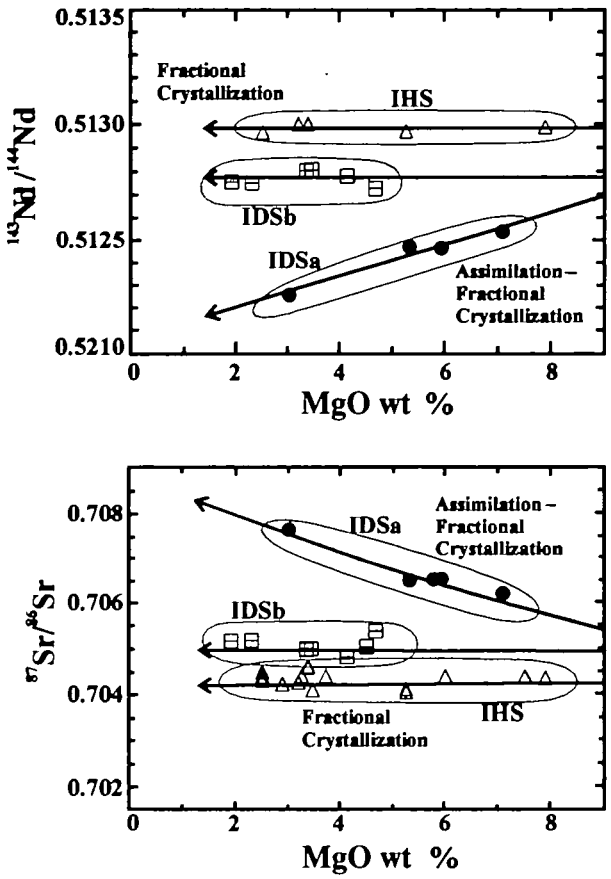

Fig. 5. Plots of MgO wt % vs $^{143}Nd/^{144}Nd$ (a) and $^{87}Sr/^{86}Sr$ (b) for representative samples of the Bequia lavas and dykes. Also shown are the fractional crystallization trends defined by the IHS and IDSb data and the open system AFC trends defined by the IDSa data. Symbols as in Fig. 2.

exceptionally high Nb content, which gives the sample a very low Zr/Nb ratio, as compared with all other IHS samples (Table 2). These high concentrations of incompatible elements, in a rock having the IHS isotopic signature, suggest that BQ1 was formed by a smaller degree of partial melting than the remainder of the suite.

There are no obvious differences in the distributions of SiO_2, CaO, Na_2O and P_2O_5 between the IHS and the IDS. The concentrations of SiO_2, Na_2O and P_2O_5 increase systematically, and CaO decreases systematically, with decreasing MgO contents. The SiO_2 and CaO trends are both characterized by an inflection at ~3·0% MgO. In the IHS, TiO_2, Al_2O_3 and K_2O contents increase systematically, and the ΣFe_2O_3 content decreases, with decreasing MgO (Table 2, Fig. 6). The K_2O and Al_2O_3 contents are higher in the IDSa than in the IHS and increase relatively systematically with decreasing MgO content (Fig. 6). In IDSa the ΣFe_2O_3 contents are lower than in the IHS and decrease systematically with MgO. In IDSb the ΣFe_2O_3 content decreases more rapidly at lower MgO contents than in the IHS or in the IDSa, and the K_2O contents are intermediate and increase with decreasing MgO content (Table 2, Fig. 6). The distribution of TiO_2 in the IDSa is similar to that of the IHS and increases systematically with decreasing MgO contents. In the IDSb the TiO_2 and Al_2O_3 distributions decrease rapidly with decreasing MgO and cross those of the IHS and the IDSa (Fig. 6).

In the IHS the Ni, Cr, and Sc contents decrease rapidly, and the V, Pb, Sr, Rb, Ba, Zr, Nb, Th, Y and the rare earth element (REE) contents increase systematically, with decreasing MgO (Tables 2 and 4, Fig. 7). The concentrations of Ni, Cr and Sc are generally lower in the IDS as compared with those of the IHS. In addition, the V, Pb, Sr, Rb, Ba, Zr, Nb, Th, Y and REE contents are systematically higher in the IDSb, and higher still in IDSa, as compared with IHS (Fig. 7, Table 2). Within each sub-suite, IDSa and IDSb, these elements follow the same general trends as they do in the IHS (Fig. 7, Table 2).

The trace element similarities and differences among the lavas are well illustrated by chondrite-normalized multi-element plots (Fig. 8). In the IHS the LREE patterns are relatively flat, $(La/Sm)_{CH}$ varies from 1·09 in the least evolved basalt to 1·34 in an andesite, and their abundances vary from ~10 to 20 times chondrite. The high field strength elements (HFSE) and heavy REE (HREE) are also characterized by relatively flat chondrite-normalized patterns, and their abundances increase from ~6·5 times chondrite in the least evolved basalt to ~18 times chondrite in the andesite (Fig. 8). Spikes in the multi-element patterns show that the IHS lavas are generally enriched in the LILE Pb, Rb, Ba, Th, K and Sr as compared with the LREE (Fig. 8). The multi-element pattern of the andesite is also characterized by the presence of a relative depletion in Ti, and the lack of enrichment in Sr relative to the HREE (Fig. 8). The more evolved basalts and the andesite have $(Pb/Yb)_{CH}$ ~1·4, indicating minor enrichment in Pb relative to the HREE (Fig. 8).

The IDSa comprises basalts with higher incompatible element concentrations, ranging from ~30 to 70 times chondrite, than the IHS. In addition, the chondrite-normalized LREE patterns show negative slopes in which La is enriched relative to Sm, and LREE abundances and relative enrichments increase from the least evolved to the most evolved basalt [$(La/Sm)_{CH}$ from 1·97 to 3·19, respectively]. The IDSa basalts have flat HFSE and HREE patterns with slightly higher concentrations, ~10–12 times chondrite, than those of the IHS (Fig. 8). Although

Downloaded from https://academic.oup.com/petrology/article/37/1/117/1530492 by guest on 21 August 2022

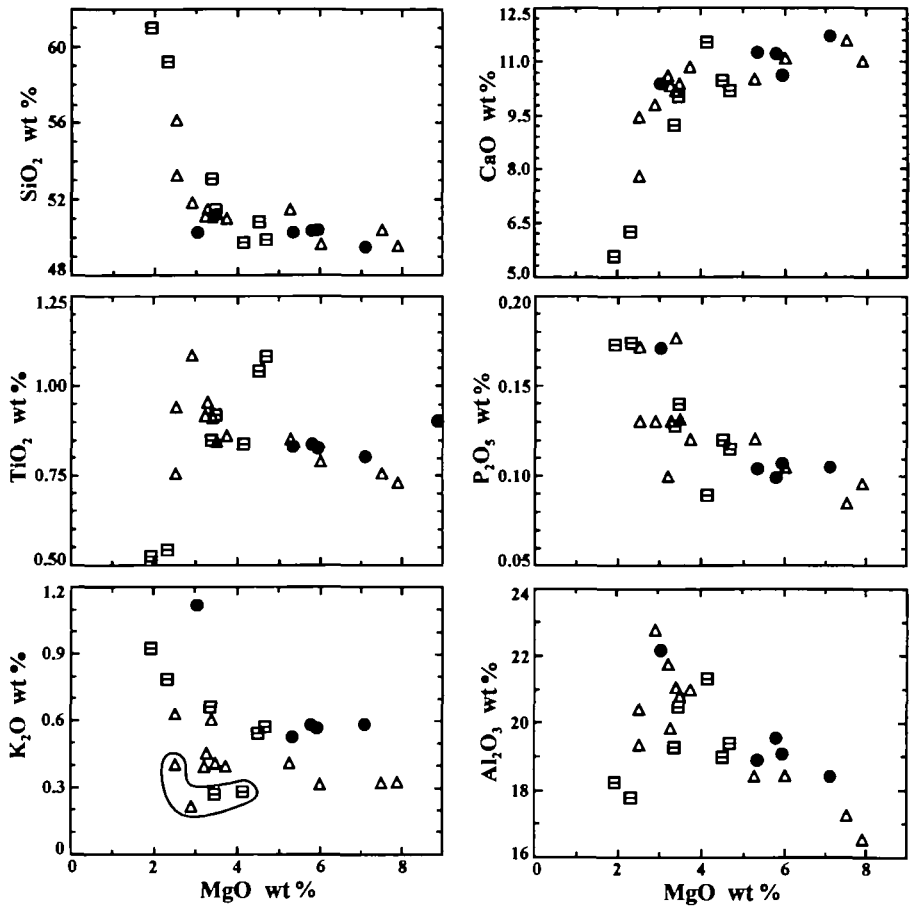

Fig. 6. Plots of SiO_2, CaO, TiO_2, P_2O_5, K_2O and Al_2O_3 variation vs MgO in the lavas and dykes of Bequia. Symbols as in Fig. 2.

the majority of the LILE are relatively enriched compared with the IHS, they do not appear as spikes on the multi-element pattern because of the greater LREE abundances and enrichments in IDSa as compared with the IHS (Fig. 8), and have higher Pb/Ce ratios (Table 2) comparable with average crustal values (0·25; Hofmann *et al.*, 1986). However, these lavas have Th (and Pb in BQ19) spikes superimposed on their LREE enrichment (Fig. 8). The IDSa lavas are all characterized by depletions in P and Ti relative to the LREE and HREE, respectively (Fig. 8). These relative depletions increase from the least evolved to the most evolved members of the suite.

The incompatible element concentrations are higher in the IDSb than they are in the IHS, but are lower than those of IDSa. The IDSb basalts also show multi-element enrichments which are intermediate between the IHS and IDSa (Fig. 8) and depletions which are similar to those of IDSa (Fig. 8). The andesite lacks the Sr spike and has a much larger negative Ti anomaly than the basalts (Fig. 8).

In summary, most of the major element concentrations and distributions are similar in the IHS and the IDSa. However, in the IDSb the total ΣFe_2O_3 content is lower and decreases more rapidly than it does in the IHS or IDSa. In addition, in the IDSb the TiO_2 and Al_2O_3 contents decrease with decreasing MgO, whereas these elements show increasing trends in the other two suites. The Ni, Cr and Sc contents tend to be lower in the IDSa and IDSb as compared with the IHS, and the incompatible element contents, including K_2O, become progressively higher from the IHS through the IDSb to the IDSa. In the IHS the relative enrichment of LILE is greater than that of the LREE as compared with the HREE. In IDSa the LILE and LREE both show approximately the same degree of enrichment relative to the HREE. IDSb samples have intermediate patterns.

Petrogenesis

The lavas are all characterized by abundant phenocrysts (>27%, Table 1) and the relatively broad

Downloaded from https://academic.oup.com/petrology/article/37/1/117/1530492 by guest on 21 August 2022

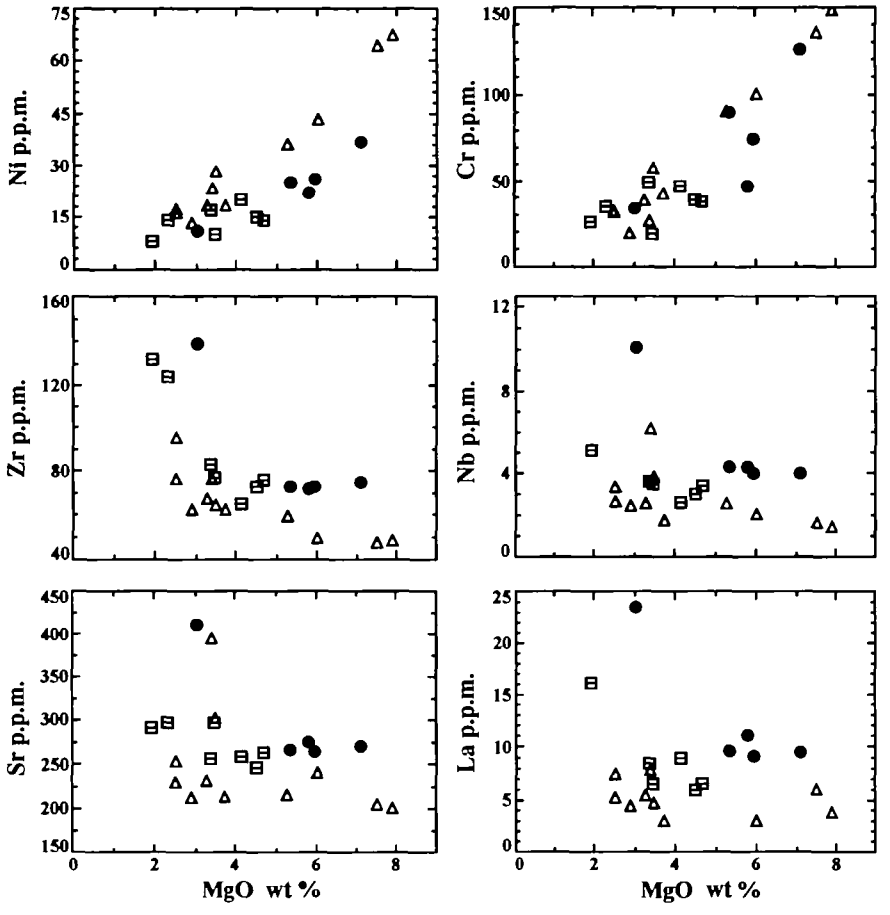

Fig. 7. Plots of variation of Ni, Cr, Zr, Nb, Sr and La contents vs MgO in the lavas and dykes of Bequia. Symbols as in Fig. 2.

trends shown by each suite on the chemical variation diagrams, for example the scatter in the Al_2O_3 in the IHS and IDSb (Fig. 6), probably result from within-suite accumulation. However, the differences in the isotope systematics among the suites rule out the possibility that all of their chemical differences can be explained by accumulation.

The increases in SiO_2, Na_2O and P_2O_5, and the decrease in CaO contents, shown by each suite are qualitatively compatible with their evolution by fractional crystallization of olivine, clinopyroxene and plagioclase. The characteristic inflection in the trends occurring at ~3% MgO is indicative of the disappearance, or significant reduction, of olivine from the fractionating assemblage (Tables 1 and 2). The most obvious difference in the evolutionary trends of the lavas is the rapid depletion of Al_2O_3, TiO_2 and ΣFe_2O_3 in the IDSb. These trends suggest that plagioclase, magnetite and perhaps amphibole are more important in the evolution of the IDSb as compared with the IHS or IDSa (Table 1).

The trace element distributions of the lavas are also qualitatively compatible with fractional crystallization of mixtures of their intratelluric minerals. For example, the rapid decrease of Ni and Cr with slowly increasing Zr, which occurs in each of the suites (Table 2), is typical of fractional crystallization of olivine and clinopyroxene, and not of partial melting. In addition, the systematic increase in incompatible element contents from the less evolved to the more evolved members of each suite is consistent with their evolution by fractional crystallization. The Ti/V ratios in the IHS range from ~16 to ~28 but do not vary systematically with TiO_2 (Table 2). There are no Ti depletions relative to other HFSE and HREE on the chondrite-normalized multi-element plots (Fig. 8) of the IHS basalts. According to Shervals (1982), such Ti–V distributions suggest that neither hornblende, which is absent from the mode, nor magnetite, which makes up <1% in the mode (Table 1), is important in the fractional crystallization of the IHS basalts. However, there is a Ti trough in the multi-element pattern of the andesite from the suite (Fig. 8) and magnetite is more abundant (>2%) in its mode

Downloaded from https://academic.oup.com/petrology/article/37/1/117/1530492 by guest on 21 August 2022

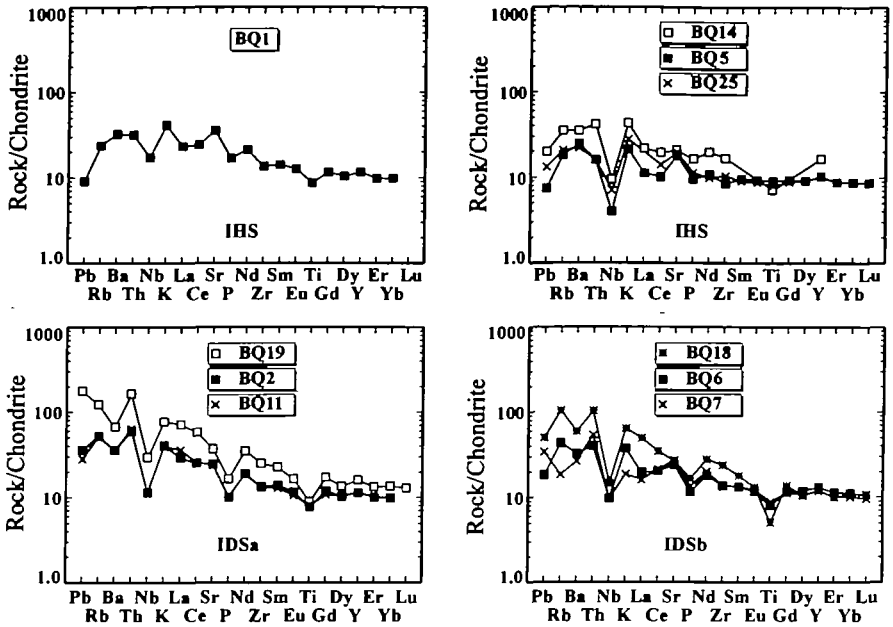

Fig. 8. Chondrite-normalized multi-element plots of representative dykes and lavas from Bequia. [Normalizing values from Sun (1980), except Rb, K and P.] Symbols as in Fig. 2.

(Table 1). Thus the chemical and mineralogical data suggest that magnetite may have entered the fractionating assemblage.

The Ti/V ratios are significantly higher in the IDS than in the IHS (Table 2). All of the IDS samples show Ti troughs in their multi-element plots which increase in size with decreasing MgO content (Fig. 8). The Ti/V ratios range from ~27 to ~97 in IDSa, and from ~22 to 64 in IDSb. These ratios do not vary systematically with TiO_2 content but tend to decrease with decreasing MgO (Table 2). Very small magnetite crystals are included in many pyroxenes and plagioclase crystals in the IDSa and IDSb basalts, suggesting that magnetite played a role in their evolution and may explain the Ti troughs in their multi-element plots.

The IHS, IDSa and IDSb lavas all have relatively flat HREE patterns, and these elements, together with Y, increase in abundance with decreasing MgO. All of the basalts have Er/Yb ratios >1, but the andesites BQ14 (IHS) and BQ18 (IDSb) have Er/Yb ratios <1 (Table 4). Amphibole is the only mineral phase capable of reducing Er relative to Yb during crystal fractionation and probably played a role in the evolution of both suites. The presence of amphibole phenocrysts in the IDSb andesite BQ20 (SiO_2 ~59%) supports this conclusion. The absence of amphibole phenocrysts in BQ14 (IHS, SiO_2 ~56·1%) and BQ18 (IDSb, SiO_2 ~61%) may be the result of pre-eruption dewatering of the magmas and subsequent resorption of the amphiboles. Thus the increase in SiO_2 during the evolution of IHS and IDSb may result from amphibole and magnetite fractionation. The conclusions which can be drawn from the major element variations in the IHS, IDSa and IDSb are consistent with the suggestion that they formed largely by fractional crystallization of similar mafic melts.

The major element variation (except K and P) of the Bequia lava suites was modelled mathematically (Table 5), using a program based on that of Wright & Doherty (1970) constrained by the intratelluric mineral assemblages of the rocks. It was possible to model the chemical variation in the IHS and IDSb fairly well (low sums of the squares of the residuals Σr^2; Table 5). However, both of the models require plagioclase accumulation and the extraction of a phenocryst assemblage very different from that actually present in the rocks (compare Tables 1 and 5). Thus neither model is regarded as satisfactory. The model for the IDSa is also rejected because it has high Σr^2 and does not fit the data well. The difficulty in producing satisfactory models for the major element variation in the Bequia lava suites supports the contention that their petrogenesis involves complex crystallization processes, including accumulation and AFC, as implied by the zoning and melt channels present in the phenocrysts, the isotopic systematics, and the relatively broad trends of chemical variation.

The isotopic evidence suggests that the magmas from which the lavas formed were derived largely

Downloaded from https://academic.oup.com/petrology/article/37/1/117/1530492 by guest on 21 August 2022

from a depleted mantle (MORB) source which had been modified by a subduction component (IHS), and that in some cases the melts had interacted with a crustal component (IDS). The importance of a MORB source is supported by the high $^{143}Nd/^{144}Nd$ of IHS lavas, and their low Nb contents (<6 p.p.m.) and Zr/Nb ratios (16·8–36·5). Differences in the concentrations and proportions of the incompatible trace elements support the suggestion that the petrogeneses of the IHS, IDSa and IDSb suites differ in detail.

The IHS and the IDS both show progressive increase in incompatible element concentrations and in LREE enrichment with decreasing MgO content (Fig. 8). The lavas all have LILE spikes, and Nb troughs in their chondrite-normalized multi-element patterns. The high Ba/La and Sr/Nd, and low Nb/La ratios, as represented by the spikes and troughs in the spidergrams (Fig. 8) of the Bequia lavas, are typical of subduction-related volcanics (Sun, 1980; Perfit *et al.*, 1980). These spikes and troughs demonstrate that the LILE (Rb, Ba, Th, K, Sr), LREE (La, Ce, Nd, Sm) and HFSE (Zr, Nb) became decoupled during the petrogenesis of the lavas and that their distribution cannot be accounted for by crystal–melt equilibria processes alone (Thompson *et al.*, 1983). The trace element decoupling is commonly attributed to the addition of a hydrous subduction component to the mantle wedge, or its melts, during arc lava genesis. The effects of crustal contamination must also be considered. Pearce (1984) has suggested a simple graphical method, which is used below (Figs 9 and 10) to distinguish trace element enrichments owing to subduction components from those derived from enriched mantle reservoirs, and possibly those owing to crustal assimilation.

The lavas of the IHS and IDS are all enriched in LILE and LREE as compared with MORB but the pattern of enrichment is different in each suite (Figs 9 and 10). The percentages of each element given in these diagrams represent the amount of the element contributed to the bulk composition of the lavas by enrichment processes. The patterns of enrichment shown by the IDSa (BQ2 and BQ19) and the IDSb (BQ6) lavas are essentially the same, and are significantly different from those shown by the IHS (Fig. 9). The least evolved basalt in the IHS (BQ5, 7·9% MgO) shows minor enrichment in Ce and then progressively greater enrichments in Pb (Fig. 8), Sr, K, Rb, Th and Ba (Fig. 9). The least evolved basalt in the IDS (BQ2, 7·1% MgO) has higher concentrations of the LILE and LREE than the BQ5, and shows progressively increasing enrichments in Ce, Sr, K, Ba, Rb, Pb (Fig. 8) and Th. Direct comparison of the patterns (Fig. 10) shows that the IDS is more enriched in Ce (LREE), K, Rb, Pb (Fig. 8) and Th than the IHS. In the IHS there is no systematic correlation between the trace element enrichment and isotopic variation. However, in the IDS the percentages of enrichment of the Ce (LREE), K, Rb, Pb and Th correlate well with the isotopic variations. For example, BQ6 from IDSb has the lowest $^{87}Sr/^{86}Sr$, $^{206}Pb/^{204}Pb$, isotopic ratios and $\delta^{18}O$ values, highest $^{143}Nd/^{144}Nd$ ratios, and the smallest percentages of enrichment, whereas the opposite is true of BQ19 (Table 2, Fig. 9). The lack of correlation between trace element enrichment and isotopic variation in the IHS, and the good correlation between these two characteristics in the IDS, implies that two separate enrichment processes are involved in the petrogenesis of the Bequia lavas. The $\delta^{18}O$ values of the IHS show that its petrogenesis was dominated by mantle processes. Thus trace element enrichment is ascribed to the addition of a subduction component to the depleted mantle wedge, producing minor increases in Ce (LREE) and Pb and progressively larger increases of Sr, K, Rb, Th and Ba (Fig. 9) in the IHS lavas. The isotopic data also suggest that IDS was formed by assimilation of progressively increasing amounts of crustal material by IHS-type melts. The correlation of the isotopic and trace element data shows that the crustal contamination leads to the addition of progressively increasing amounts of Ce (LREE), K, Rb, Pb and Th (Fig. 9). Thus the trace element data support the interpretation of the isotopic data that the genesis of the Bequia lavas involves the depleted mantle, a subduction component and a crustal component.

DISCUSSION

The components which may contribute to the final composition of island arc volcanics, including those of the Lesser Antillean arc, are depleted (MORB) or enriched (OIB) mantle, subducted oceanic crust including sediment and dehydration fluids or melt, and intracrustal sediment (Thirlwall & Graham, 1984; Davidson, 1986; White & Dupré, 1986; Ben Othman *et al.*, 1989). Many aspects of the petrogenesis of volcanic arc lavas are poorly understood, including the nature of the mantle wedge above subduction zones, the nature, composition and magnitude of the subduction zone components, and the flux ratio of mantle-derived mass to recycled crust (Hawkesworth *et al.*, 1993).

It has been shown that the genesis of the Bequia lavas involves depleted mantle, a subduction component and a crustal component. Within this

Downloaded from https://academic.oup.com/petrology/article/37/1/117/1530492 by guest on 21 August 2022

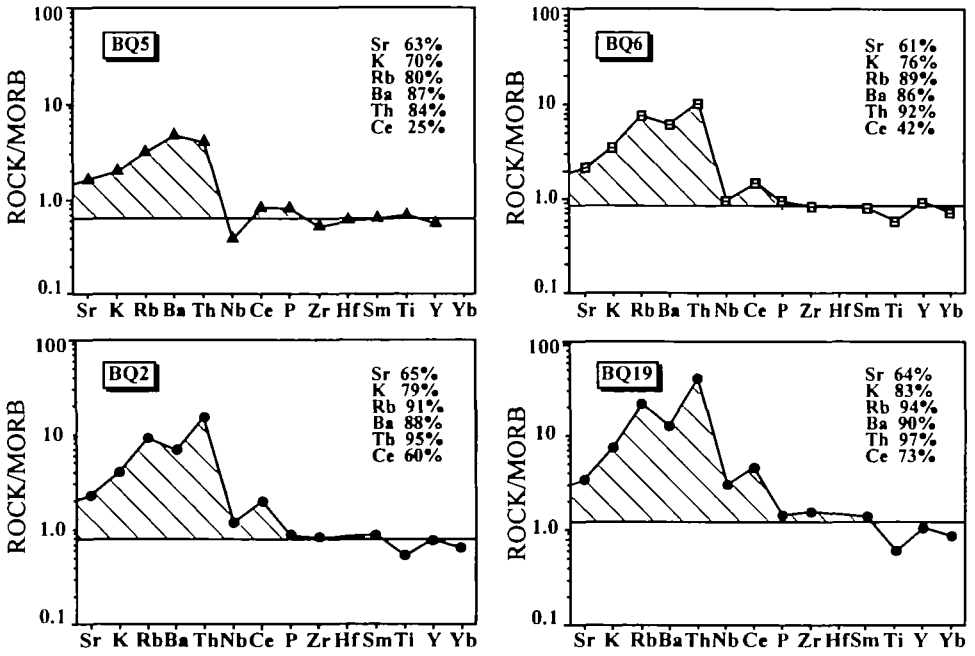

Fig. 9. MORB-normalized multi-element plots of BQ5 (IHS), BQ6 (IDSb), BQ2 (IDSa) and BQ19 IDSa. Hatched areas indicate elemental enrichments as compared with MORB [normalizing values Pearce (1984)].

framework, the data presented above may be utilized to improve our understanding of some of the problems relating to island arc lavas. Below, we attempt to use the differences between the isotopic compositions and trace element patterns of MORB and the IHS basalts to place some constraints on the composition, nature and amount of the subduction component, as well as the process by which it was added to the lavas. In addition, the differences between the isotopic compositions and trace element patterns of the IHS and the IDS are used in an effort to place some constraints on the amount, nature and composition of the crustal component as well as the process by which it was added.

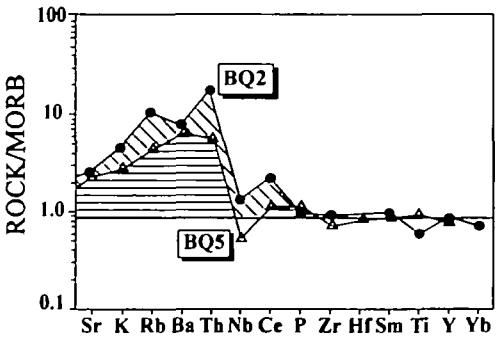

Fig. 10. MORB-normalized plot comparing the different patterns of enrichment characteristic of BQ5 (IHS) and BQ2 (IDSa) at approximately the same MgO value.

The subduction component

The subduction component involved in the petrogenesis of the Bequia lavas is enriched in several of the LILE, and shows minor enrichment in the LREE and Pb. It has been suggested that subduction components are (siliceous) hydrous fluids or hydrous anatectic melts, formed during the dehydration of the downgoing slab (Gill, 1981; Hole *et al.*, 1984; Tatsumi *et al.*, 1986; Morris, 1989; Bebout, 1991; McDonough, 1991), or bulk sediment (White & Dupré, 1986), and may comprise a mixture of more than one component (Hawkesworth *et al.*, 1993).

The pattern of LILE and LREE enrichment, as compared with depleted mantle, estimated for the subducted sediments based on data from DSDP Hole 543 (enrichment factors Sr 6×, Nd 30×, Ba 40×, Ce 60×, K 60×, Pb and Th 150× MORB; White & Dupré, 1986) is different from that produced by the subduction component in the Bequia lavas (Fig. 9). This precludes the possibility that bulk mixing between sediment and the mantle accounts for all of the subduction modification [see also Davidson (1987)].

The IHS lavas have higher Sr, Pb and Nd contents and the Sr/Nd ratios (2–3×, 2–6×, 1–2× and 1·5–2×, respectively) than MORB (Table 2). They also have higher $^{87}Sr/^{86}Sr$ and radiogenic Pb, and slightly lower $^{143}Nd/^{144}Nd$ ratios than MORB and the depleted mantle. The high Sr/Nd ratios in the

Downloaded from https://academic.oup.com/petrology/article/37/1/117/1530492 by guest on 21 August 2022

IHS basalts are believed to result from the addition of a subduction component and not from plagioclase resorption, as described by Vukadinovic (1993) for many oceanic arc basalts, because the Sr contents increase systematically with the $^{87}Sr/^{86}Sr$ ratios. Thus it is suggested that the subduction component had higher concentrations of Sr, Pb and Nd, and higher Sr/Nd ratios than the IHS lavas. In addition, it must have more radiogenic Sr and Pb isotope ratios, and lower $^{143}Nd/^{144}Nd$ ratios, than either depleted mantle or the lavas. As discussed below, the subduction component must comprise contributions from subducted sediments, which have high $^{87}Sr/^{86}Sr$, radiogenic Pb and $\delta^{18}O$, and low $^{143}Nd/^{144}Nd$ and Sr/Nd ratios, and from altered mafic crust, which has high $^{87}Sr/^{86}Sr$, $^{143}Nd/^{144}Nd$ and Sr/Nd ratios (O'Nions *et al.*, 1978; White, 1985; Ben Othman *et al.*, 1989; Hawkesworth *et al.*, 1993), to account for the isotopic and trace element variation of the IHS lavas.

All of the lavas are characterized by negative Ce anomalies on chondrite-normalized diagrams (Ce/Ce* in the IHS 0·80–0·92, in the IDSa 0·79–0·94, in the IDSb 0·82–0·95), which are a characteristic feature of deep ocean water (Goldberg *et al.*, 1963). Their presence in the lavas suggests that the anomalies result from the addition of the subduction component to the mantle. The mafic crust in subducting slabs has been altered by interaction with seawater, and the overlying sediments also contain significant quantities of seawater. We suggest that the subduction component is largely made up of a fluid derived from the original seawater which was released by dehydration of subducted mafic crust and sediments under oxidizing conditions. Under these conditions, tetravalent Ce will be preferentially included in the slab minerals, thus accentuating the original Ce anomaly. The distribution of LILE and LREE between hydrous fluids and the subducting slab cannot be estimated because of the lack of experimentally determined partition coefficients, but the fluids are expected to contain higher concentrations of soluble LILE (Ba, Sr) and lower concentrations of the less soluble LREE (Ce) (Weaver, 1991).

Bebout (1991) noted that 'Petrologic relations and trace element and isotopic systematics in arc volcanic rocks suggest that water-rich fluids flux partial melting in the source regions of arc magmatism (depths of 80 to 150 km) and contribute slab-derived chemical components to such regions (radiogenic isotopic signatures of Pb, Sr, and Be and trace elements)' but did not discuss the source of the fluids. Fluids formed by dehydration of altered MORB crust are estimated to have 240 p.p.m. Rb, 110 p.p.m. Sr and 520 p.p.m. Ba, extremely low contents of REE (Hole *et al.*, 1984; Table 2), $^{87}Sr/^{86}Sr$ ~0·704, $^{143}Nd/^{144}Nd$ ~0·51311 and $^{206}Pb/^{204}Pb$ ~18·46 (O'Nions, 1984). The Sr and Pb isotope ratios of these fluids are too low, and the Nd isotope ratios are too high, to explain the radiogenic isotope ratios of the IHS ($^{87}Sr/^{86}Sr$ 0·70460, $^{143}Nd/^{144}Nd$ 0·512960, $^{206}Pb/^{204}Pb$ 19·511; Table 3). This suggests that an additional contribution must be made to the subduction component.

Studies of the ^{10}Be and B distributions in modern arc volcanics suggest that aqueous fluids (or possibly melts) of constant composition, probably derived from sediments with or without the altered oceanic crust, are released during dehydration of the slab. These rise into the mantle wedge, causing metasomatism and possibly melting (Morris *et al.*, 1990). The involvement of sediments in the petrogenesis of the volcanic arc lavas of the Lesser Antilles is also indicated by the fact that the $(Ba/La)_N$ ratios of the lavas and hemipelagic sediments (0·83) are characteristically lower than those of other oceanic arcs (Ben Othman *et al.*, 1989). The dominantly hemipelagic sediments which occur in front of the Lesser Antillean arc have other trace element and isotopic characteristics which provide further support for this contention. Like Pacific pelagic sediments (Hole *et al.*, 1984), they have relatively high LILE and LREE contents and low HREE and HFSE contents as compared with those of altered oceanic crust as well as high $^{87}Sr/^{86}Sr$ (0·7095–0·7170) and $^{206}Pb/^{204}Pb$ (18·8–19·4) and low $^{143}Nd/^{144}Nd$ (0·51200–0·51215) ratios (White & Dupré, 1986; Ben Othman *et al.*, 1989). Fluids or melts derived from these sediments would contain the necessary elements and isotopes to modify the mantle source from which the IHS is derived. The lavas of the IHS have high Pb/Ce ratios relative to MORB, which also imply that sediments played a role in the lava petrogenesis (Hole *et al.*, 1984; Ben Othman *et al.*, 1989). The $(La/Sm)_N$ ratios of the IHS are higher for any given Zr/Nb ratio than those of oceanic basalts, suggesting that some of the LREE were supplied by the subduction component. We conclude that at least some of the LREE budget of the Bequia lavas contributed by the subduction component is derived from the sediments [see also Gill (1981), Hole *et al.* (1984), Davidson (1986), White & Dupré (1986) and Ben Othman *et al.* (1989)]. The relatively high radiogenic Pb isotopic ratios and their trends in the lavas also support the contention that Pb from the sediments is present in the subduction component [see also Bebout (1991)].

The physical conditions present during dehydration of the slab (<700°C and <20 kbar) should cause the sediments, but not the mafic part of the

Downloaded from https://academic.oup.com/petrology/article/37/1/117/1530492 by guest on 21 August 2022

subducting slab (Peacock, 1990; McCulloch, 1993), to partially melt (minimum water-saturated melting >600°C and ~15 kbar; Wyllie *et al.*, 1976). Some of the resultant hydrous siliceous melts may become entrained in the convecting mantle wedge, because of their high viscosity, and may be carried down to ~150 km, at which depth the hydrated mantle undergoes pressure-controlled dehydration (Tatsumi, 1989). The limited range of isotopic ratios shown by the lavas of the IHS (Table 3) suggests that the effects of the addition of the subduction component to the mantle are relatively homogeneous. This can be explained if the siliceous melts are incorporated into much larger volumes of mafic melt generated as dehydration volatiles, released at this depth, flux the mantle.

The addition of fluids and melts derived from subducted sediments and mafic crust is adequate to account for the high LILE and moderate LREE contents, the high Ba/La, Sr/Nd, Pb/Ce and La/Nb, and elevated radiogenic Sr and Pb ratios of the IHS lavas. We conclude that the IHS was derived from a depleted mantle source modified by bulk mixing with a subduction component derived from the downgoing slab.

The petrogenetic evolution of the IHS suggested above was modelled using various percentages of mantle and subduction components, and various crust and mantle isotopic and elemental ratios. The models were constrained by compositions of depleted mantle (Davidson, 1986; White & Dupré, 1986) and subduction components comprising dehydration fluids (O'Nions *et al.*, 1978; Bebout, 1991), and locally subducting sediments (White & Dupré, 1986) (Table 6). The majority of the $^{206}Pb/^{204}Pb$ ratios of the sediments are lower than those of the IHS lavas and could not satisfy the mixing requirements. The negligible difference in $\delta^{18}O$ values between the mantle and the IHS lavas strongly implies that this value must be relatively low in the subduction component. For example, a 2% addition of a subduction component with $\delta^{18}O = 15$ yields a value of ~5·9 for the modified mantle, which is higher than the values measured in the IHS. The isotopic ratios used for the sediment were in the range 0·709–0·7170 for $^{87}Sr/^{86}Sr$, 0·5125–0·5120 for $^{143}Nd/^{144}Nd$ and 19·8 for $^{206}Pb/^{204}Pb$, and $\delta^{18}O$ values ranged from 15, taken from fluids generated during the subduction of the Catalina Schist (Bebout, 1991), to eight, from a metamorphosed limestone block from St Vincent which also had an $^{87}Sr/^{86}Sr$ of 0·7077 (M. F. Thirlwall, J. P. Davidson & R. S. Harmon, unpublished data).

In the absence of known trace element and isotopic compositions of the subduction component, the results of such modelling cannot be definitive. However, the high $^{143}Nd/^{144}Nd$ ratios and low $\delta^{18}O$ values of the IHS lavas show that they were dominantly derived from depleted mantle. The composition of depleted mantle is moderately well known; thus a wide range of possible subduction component compositions were tested. Calculations using the isotopic constraints described above suggest that the IHS could be formed by partial melting of depleted mantle which has been modified by the addition of a small percentage (1–4%) of a subduction component, containing low concentrations of Sr (50–200 p.p.m.), Nd (2–10 p.p.m.) and Pb (3–5 p.p.m.), and having an Sr/Nd ratio higher than those of the subducting sediments (Table 6).

The $^{87}Sr/^{86}Sr$ ratio of 0·709 was selected for the preferred model, from the matrix of calculations, because the negative Ce anomalies (Ce/Ce* 0·80–0·92) in the chondrite-normalized trace element patterns of the IHS lavas (Fig. 8) are indicative of an important role for seawater ($^{87}Sr/^{86}Sr$ ~0·7091; O'Nions, 1984) in the genesis of the IHS. The relatively low concentrations of Sr, Nd and Pb required by the subduction component in all of these models (Table 6) also support its origin as being largely from original seawater. Appropriate $^{143}Nd/^{144}Nd$ and $^{206}Pb/^{204}Pb$ ratios, $\delta^{18}O$ values, and Sr, Nd and Pb contents were selected from the calculations (Table 6) to provide the best fit of the model to the measured data (Curve A, Figs 2 and 4). The resultant preferred model involves the mixing of ~3% of a subduction component (Sr 110 p.p.m., $^{87}Sr/^{86}Sr$ 0·709, Nd 2 p.p.m., $^{143}Nd/^{144}Nd$ 0·51210, Pb 4 p.p.m., $^{206}Pb/^{204}Pb$ 19·8, $\delta^{18}O$ 10‰) with depleted mantle. The low $\delta^{18}O$ required for this model may be the result of subduction zone metamorphism or may indicate that part of the oxygen, like the Sr, was derived from the mafic crust. The model is also characterized by internally consistent trace elemental ratios, is in accord with the major element changes in the suite, and is petrogenetically reasonable.

The crustal component

The IDS lavas were formed from IHS-type melts which assimilated progressively increasing amounts of (possibly) Precambrian crustal material. The phenocryst assemblages of the IDS imply that the AFC occurred at depths of <10 km. The Orinoco river has been delivering sediments from the Guyana Shield to this area in the southern Lesser Antilles continuously since the Cretaceous, and it is possible that the volume delivered in the past was greater than at present (White & Dupré, 1986). The crust

Downloaded from https://academic.oup.com/petrology/article/37/1/117/1530492 by guest on 21 August 2022

beneath Bequia is relatively thick (~20 km; Speed & Walker, 1991), and Bouysse (1988) has recently presented some evidence that the southern part of the Lesser Antillean arc may be underlain by Mesozoic crust. Thus abundant fine-grained sediments derived from the Guyana Shield may occur, in the arc crust beneath Bequia, at an appropriate depth to take part in the AFC process.

Precambrian gneisses from the Guyana Highlands have highly radiogenic Pb with average reported $^{206}Pb/^{204}Pb$ ratios of ~20·5 (Montgomery, 1979). Fine-grained sediments derived from these gneisses would have similar Pb isotopic ratios and the assimilation of such sediments by IHS-type melts would give rise to the high Pb isotopic ratios which are characteristic of the IDS lavas (Table 3). No estimates of the average chemical composition of the fine-grained sediments derived from the Guyana Shield are available. However, the compositions of Post-Archaean shales from several major shields have been estimated (Taylor & McClennan, 1985) and all are characterized by high K_2O, LREE, Pb, Rb and Th, and relatively low ΣFe_2O_3, MgO, Ni and Cr. The chemical compositions of fine-grained sediments derived from the Guyana Shield are likely to be similar to those of the uniform shales representative of other major shields; AFC involving such shales would cause enrichment of IHS melts in K_2O, LREE, Pb, Rb and Th, and depletion in Ni and Cr, a pattern which is similar to that seen in the IDS lavas (Table 2, Fig. 10).

The variations in radiogenic isotopic ratios and trace element contents in the IDS were modelled using equations derived for assimilation–fractional crystallization by DePaolo (1981*a*). The variation in $\delta^{18}O$ was modelled using the method outlined by Taylor (1980). All models were constrained by the isotopic ratios and trace element contents of the IHS as one of the components involved in the AFC. Curves fitted to the $^{206}Pb/^{204}Pb$ vs $^{87}Sr/^{86}Sr$ and $^{206}Pb/^{204}Pb$ vs $^{143}Nd/^{144}Nd$ ratios tend to become asymptotic at $^{206}Pb/^{204}Pb$ ratios ~20·4 (Fig. 4). This ratio is similar to the average $^{206}Pb/^{204}Pb$ of the Guyana Shield gneisses and was taken as a first approximation of the $^{206}Pb/^{204}Pb$ ratio of the assimilant. No $^{87}Sr/^{86}Sr$ or $^{143}Nd/^{144}Nd$ ratios are available for the sediments derived from the Guyana Shield but the average Precambrian crust has $^{143}Nd/^{144}Nd$ ratios $\leqslant$0·5115 (DePaolo, 1981*b*) together with $^{87}Sr/^{86}Sr$ ratios which may range up to 0·720 or more (Faure, 1986). The Sr and Nd isotope ratios of the IDS lavas lie on a shallow curve from which paired ratios of $^{87}Sr/^{86}Sr$ and $^{143}Nd/^{144}Nd$, between 0·709 and 0·5114 and 0·720 and 0·5090, were tested with $\delta^{18}O$ values between 10 and 30, and Sr/O and Nd/O melt:crust ratios ranging between 0·2 and 1·0. There is no unique solution to this mixing problem; however, it is possible to construct an internally consistent model (Curve B, Figs 2 and 4, and Fig. 11) which suggests that the AFC interpretation of the origin of the IDS is reasonable. The model shows that the IDSa lavas could be formed by 30–55% fractional crystallization during the assimilation of a crustal component characterized by 490 p.p.m. Sr, $^{87}Sr/^{86}Sr$ ~0·713, 23 p.p.m. Nd, $^{143}Nd/^{144}Nd$ ~0·5112, Pb 35 p.p.m. $^{206}Pb/^{204}Pb$ ~20·4 and $\delta^{18}O$ ~15‰ (see Table 7 for full details). The $^{143}Nd/^{144}Nd$ ratio which is chosen for the preferred model is lower than the value typical of the sediments from DSDP Hole 543 (0·5121; White & Dupré, 1986). This implies that the older hemipelagic sediments, deeper in the section, contain a greater proportion of terrestrially derived material than the younger analysed sediments [see also White & Dupré (1986)]. The IDSb lavas show two stages

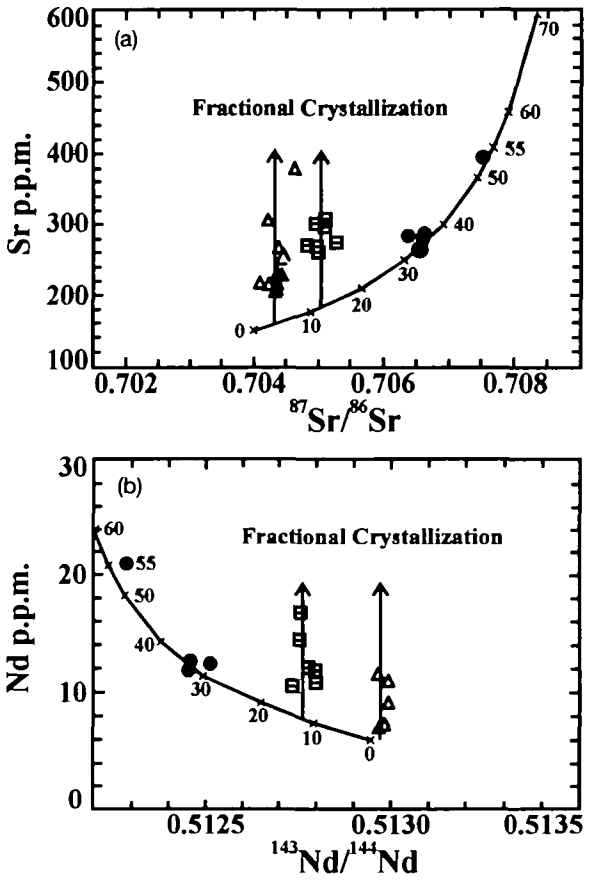

Fig. 11. Plots showing variation of $^{87}Sr/^{86}Sr$ ratios vs Sr p.p.m. (a) and $^{143}Nd/^{144}Nd$ ratios vs Nd p.p.m. (b) for selected IHS and IDS samples together with the assimilation–fractional crystallization curve defined by the preferred model for the genesis of the IDSa lavas. Symbols as in Fig. 2.

Downloaded from https://academic.oup.com/petrology/article/37/1/117/1530492 by guest on 21 August 2022

in their evolution. In the first stage, the Sr and Nd contents and $^{87}Sr/^{86}Sr$ ratios increase, and $^{143}Nd/^{144}Nd$ ratios decrease, during 10–18% assimilation–fractional crystallization. This is followed by increases in Sr and Nd contents at constant isotopic ratios (Fig. 11) which may be representative of either closed system fractional crystallization or AFC in which there is no isotopic contrast between the melt and the assimilant.

All of the lavas are very similar petrographically, in their phenocryst assemblages and compositional zoning, and in their major element geochemistry. Thus they appear to have undergone very similar petrogenetic processes, and we favour the view that they tend to develop in long-lived magma chambers in the sub-arc crust. Hildreth & Moorbath (1988) suggested that closed system fractional crystallization of basaltic magmas in the crust is probably very rare, and that AFC is the dominant process. Where there is no isotopic evidence of assimilation, those workers suggested that newly emplaced melts have probably interacted with isotopically similar rocks previously crystallized on the magma chamber walls. DePaolo *et al.* (1992) have pointed out that the amount of assimilation is governed by the ambient temperature of the crust and the rate of supply of magma. Where the crustal temperature is high there is greater crustal assimilation, and when the magma supply is high the crustal contribution is diluted. The Bequia lavas require progressively increasing amounts of crustal assimilation to explain the isotopic ratios of the IHS, IDSb, and IDSa. The differences in the evolution of the IHS (no crustal assimilation), the IDSb (minor crustal assimilation followed by apparent closed system fractionation) and the IDSa (abundant crustal assimilation) are best explained if variation in the magma supply, variation in the ambient crustal temperature and large quantities of crystals coating the magma chamber walls during assimilation all affected the Pliocene magma chambers which were present beneath Bequia.

CONCLUSIONS

Two suites of lavas and dykes can be identified on the island of Bequia, each comprising dominantly basalts with a few andesites. The incompatible element contents and isotopic ratios of the IHS suggest that it was derived from a depleted mantle source which was contaminated by hydrous fluids and minor siliceous melts formed during the dehydration of subducted sediments and mafic crust. The IDS lavas formed from melts similar in chemical and isotopic composition to those of the IHS which interacted with crustal sediments, probably largely derived from the Precambrian Guyana Shield, by assimilation–fractional crystallization.

ACKNOWLEDGEMENTS

Radiogenic and stable isotope, and X-ray fluorescence facilities at Royal Holloway are London University Intercollegiate Research Services, and we thank Gerry Ingram, Dave Mattey and Giz Marriner for their assistance. T.E.S. wishes to thank the Natural Sciences and Engineering Research Council of Canada for providing funds for this study. Drs. Jon Davidson and Simon Turner are thanked for very helpful reviews of the original manuscript.

REFERENCES

Bebout, G. E., 1991. Geometry and mechanisms of fluid flow at 15 to 45 kilometer depths in an early Cretaceous accretionary complex. *Geophysical Research Letters* **18**, 923–926.

Ben Othman, D., White, W. M. & Patchett, J., 1989. The geochemistry of marine sediments, island arc magma genesis, and crust–mantle recycling. *Earth and Planetary Science Letters* **94**, 1–21.

Bouysse, P., 1988. Opening of the Grenada back-arc basin and the evolution of the Caribbean plate during the Mesozoic and Early Paleogene. *Tectonophysics* **149**, 121–143.

Briden, J. C., Rex, D. C., Faller, A. M. & Tomblin, J. F., 1979. K–Ar geochronology and palaeomagnetism of volcanic rocks in the Lesser Antilles island arc. *Philosophical Transactions of the Royal Society of London, Series A* **291**, 485–528.

Cas, R. A. F. & Wright, J. V., 1987. *Volcanic Successions Modern and Ancient*. London: Allen and Unwin, 528 pp.

Davidson, J. P., 1983. Lesser Antilles isotopic evidence of the role of subducted sediments in island arc magma genesis. *Nature* **306**, 253–256.

Davidson, J. P., 1985. Mechanisms of contamination in Lesser Antilles island arc magmas from radiogenic and oxygen isotopic relationships. *Earth and Planetary Science Letters* **72**, 163–174.

Davidson, J. P., 1986. Isotopic and trace element constraints on the petrogenesis of subduction-related lavas from Martinique, Lesser Antilles. *Journal of Geophysical Research* **91**(B6), 5943–5962.

Davidson, J. P., 1987. Crustal contamination versus subduction zone enrichment: examples from the Lesser Antilles and implications for mantle source compositions of island arc volcanic rocks. *Geochimica et Cosmochimica Acta* **51**, 2185–2198.

Davidson, J. P. & Harmon, R. S., 1989. Oxygen isotopic constraints on the petrogenesis of volcanic arc magmas from Martinique, Lesser Antilles. *Earth and Planetary Science Letters* **95**, 255–270.

Davidson, J. P., Boghossian, N. D. & Wilson, M., 1993. The geochemistry of the igneous rock suite of St Martin, Northern Lesser Antilles. *Journal of Petrology* **34**, 839–866.

DePaolo, D. J., 1981*a*. Trace element and isotopic effects of combined wallrock assimilation and fractional crystallization. *Earth and Planetary Science Letters* **53**, 189–202.

DePaolo, D. J., 1981*b*. A neodymium and strontium isotopic study of the Mesozoic calc-alkaline granitic batholiths of the Sierra Nevada and Peninsular Ranges, California. *Journal of Geophysical Research* **86**, 10470–10488.

DePaolo, D. J., Perry, F. V. & Baldridge, W. S., 1992. Crustal versus mantle sources of granitic magmas: a two parameter

Downloaded from https://academic.oup.com/petrology/article/37/1/117/1530492 by guest on 21 August 2022

model based on Nd isotopic studies. *Transactions of the Royal Society of Edinburgh* **83**, 439–446.

Faure, G., 1986. *Principles of Isotope Geology*, 2nd edn. New York: John Wiley, 589 pp.

Ford, C. E., Russell, D. G., Craven, J. A. & Fisk, M. R., 1983. Olivine–liquid equilibria: temperature, pressure and composition dependence of the crystal/liquid cation partition coefficients of Mg, Fe^{2+}, Ca and Mn. *Journal of Petrology* **24**, 256–265.

Gill, J., 1981. *Orogenic Andesites and Plate Tectonics*. Berlin: Springer-Verlag, 390 pp.

Goldberg, E. D., Koide, M., Schmitt, R. A. & Smith, R. H., 1963. Rare-earth distributions in marine environment. *Journal of Geophysical Research* **68**, 4209–4217.

Green, T. H., 1982. Anatexis of mafic crust and high pressure crystallization of andesite. In: Thorpe, R. S. (ed.) *Andesites*. Chichester: John Wiley, pp. 465–487.

Hanson, G. N. & Langmuir, C. H., 1978. Modelling of major elements in mantle–melt systems using trace element approaches. *Geochimica et Cosmochimica Acta* **42**, 725–742.

Hart, S R., 1984. A large-scale isotope anomaly in the Southern Hemisphere mantle *Nature* **509**, 753–757.

Hawkesworth, C. J , Gallagher, K., Hergt, J. M. & McDermott, F., 1993. Mantle and slab contributions in arc magmas. *Annual Reviews in Earth and Planetary Science* **21**, 175–204.

Hildreth, W. & Moorbath, S., 1988. Crustal contributions to arc magmausm in the Andes of central Chile. *Contributions to Mineralogy and Petrology* **98**, 455–489.

Hofmann, A. W., Jochum, K. P., Seufert, M. & White, W. M., 1986. Nb and Pb in oceanic basalts: new constraints on mantle evolution. *Earth and Planetary Science Letters* **79**, 33–45.

Hole, M. J., Saunders, A. D., Marriner, G. F. & Tarney, J., 1984. Subduction of pelagic sediments: implications for the origin of Ce-anomalous basalts from the Mariana Islands. *Journal of the Geological Society, London* **141**, 453–472.

James, D. E., 1981. The combined use of oxygen and radiogenic isotopes as indicators of crustal contamination. *Annual Reviews, Earth and Planetary Science* **9**, 311–344.

Kalamarides, R. I., 1986. High-temperature oxygen isotope fractionation among the phases of the Kiglapait Intrusion, Labrador, Canada. *Chemical Geology (Isotope Geoscience Section)* **58**, 303–310.

Kyser, T. K., 1990. Stable isotopes in the continental lithospheric mantle. In: Menzies, M. (ed.) *Continental Mantle*. Oxford: Oxford Science, pp. 127–156.

Mattey, D. P. & Macpherson, C. M., 1993. High precision oxygen isotope microanalysis of ferromagnesian minerals by laser-fluorination. *Chemical Geology (Isotope Geoscience Section)* **105**, 305–318.

Mattey, D. P., Lowry, D. & Macpherson, C. G., 1994. Oxygen isotope compositions of mantle peridotites. *Earth and Planetary Science Letters* **128**, 231–241.

McCulloch, M. T., 1993. The role of subducted slabs in an evolving earth *Earth and Planetary Science Letters* **115**, 89–100.

McDonough, W. F., 1991. Partial melting of subducted oceanic crust and isolation of its residual eclogitic lithology. *Philosophical Transactions of the Royal Society of London* **335**, 181–192.

Montgomery, C., 1979. Uranium–lead geochronology of the Archean Imataca Series, Venezuelan Guyana Shield. *Contributions to Mineralogy and Petrology* **64**, 167–176.

Morris, J., 1989. Subduction, volcanism, and change in the earth. *Carnegie Institution of Washington Yearbook* **88**, 116–122.

Morris, J., Leeman, W. P. & Tera, F., 1990. The subducted component in island arc lavas: constraints from Be isotopes and B–Be systematics. *Nature* **344**, 31–36.

O'Nions, R. K., 1984. Isotopic abundances relevant to the identification of magma sources. *Philosophical Transactions of the Royal Society of London, Series A* **301**, 591–603.

O'Nions, R. K., Carter, S. R., Cohen, R. S., Evensen, N. W. & Hamilton, P. J., 1978. Pb, Nd, and Sr isotopes in oceanic ferromanganese deposits and ocean floor basalts. *Nature* **273**, 435–438.

Peacock, S. M., 1990. Fluid processes in subduction zones. *Science* **248**, 329–337.

Pearce, J. A., 1984. Role of the sub-continental lithosphere in magma genesis at active continental margins. In: Hawkesworth, C. J. & Norry, M. J. (eds) *Continental Basalts and Mantle Xenoliths*. Nantwich, UK: Shiva, pp. 230–249.

Perfit, M. R., Gust, D. A., Bence, A. E., Arculus, R. J. & Taylor, S. R., 1980. Chemical characteristics of island arc basalts: implications for mantle sources. *Chemical Geology* **30**, 227–256.

Shervais, J. W., 1982. Ti–V plots and the petrogenesis of modern and ophiolitic lavas. *Earth and Planetary Science Letters* **59**, 101–118.

Speed, R. A. & Walker, J. A., 1991. Oceanic crust of the Grenada Basin in the Southern Lesser Antilles Arc Platform. *Journal of Geophysical Research* **96**(B3), 3835–3851.

Sun, S.-S., 1980. Lead isotopic study of young volcanic rocks from mid-ocean ridges, ocean islands and island arcs. *Philosophical Transactions of the Royal Society of London, Series A* **297**, 409–445.

Tatsumi, Y., 1989. Migration of fluid phases and genesis of basalt magmas in subduction zones. *Journal of Geophysical Research* **94**, 4697–4707.

Tatsumi, Y., Hamilton, D. L. & Nesbitt, R. W., 1986. Chemical characteristics of fluid phase released from subducted lithosphere and origin of arc magmas: evidence from high-pressure experiments and natural rocks. *Journal of Volcanology and Geothermal Research* **29**, 293–309.

Taylor, H. P., Jr, 1980. The effects of assimilation of country rock by magmas on $^{18}O/^{16}O$ and $^{87}Sr/^{86}Sr$ systematics in igneous rocks. *Earth and Planetary Science Letters* **47**, 243–254.

Taylor, S. R. & McClennan, S. M., 1985. *The Continental Crust: its Composition and Evolution*. Oxford: Blackwell Scientific, 312 pp.

Thirlwall, M. F., 1982. A triple filament method for rapid and precise analysis of rare-earth elements by isotope dilution. *Chemical Geology* **35**, 155–166.

Thirlwall, M. F. & Graham, A. M., 1984. Evolution of high-Ca, high-Sr C-series basalts from Grenada, Lesser Antilles: the effects of intra-crustal contamination. *Journal of the Geological Society of London* **141**, 427–445.

Thirlwall, M. F., Smith, T. E., Graham, A. M. & Davidson, J. P., 1991. Constraints on the origin of arc lava HFSE anomalies from basalts of the Lesser Antilles. *Terra Abstracts* **3**, 44.

Thirlwall, M. F., Smith, T. E., Graham, A. M., Theodorou, P., Hollings, P., Davidson, J. P. & Arculus, R. J., 1994. High field strength element anomalies in arc lavas, source or process? *Journal of Petrology* **35**, 819–838.

Thirlwall, M. F., Lowry, D., MacPherson, C. G., Smith, T. E., Arculus, R. J. & Graham, A. M., 1995. Laser fluorination oxygen isotope geochemistry of the southern Lesser Antilles Arc. *Terra Abstracts* **7**, 229.

Thompson, R. N., Morrison, M. A., Dickin, A. P. & Hendry, G. L., 1983. Continental flood basalts . . . arachnids rule OK? In: Hawkesworth, C. J. & Norry, M. J. (eds) *Continental Basalts and Mantle Xenoliths*. Nantwich, UK: Shiva, pp. 158–185.

Vroon, P. Z., van Bergen, M. J., White, W. M. & Varekamp, J. C., 1993. Sr–Nd–Pb isotope systematics of the Banda Arc, Indonesia: combined subduction and assimilation of continental material. *Journal of Geophysical Research* **98**, 22349–22366.

Downloaded from https://academic.oup.com/petrology/article/37/1/117/1530492 by guest on 21 August 2022

Vukadinovic, D., 1993. Are Sr enrichments in arc basalts due to plagioclase accumulation? *Geology* **21**, 123–126.

Weaver, B. L., 1991. Trace element evidence for the origin of ocean-island basalts. *Geology* **19**, 123–126.

Westercamp, D., Andreieff, P., Bouysse, P., Mascle, A. & Baubron, J-C., 1985. Géologie de l'archipel des Grenadines (Petites Antilles Méridionales). Étude monographique. *Documents du Bureau de Recherches Géologiques et Minières* **92**, 198 pp.

White, W. M., 1985. Sources of oceanic basalts: radiogenic isotope evidence. *Geology* **13**, 115–118.

White, W. M. & Dupré, B., 1986. Sediment subduction and magma genesis in the Lesser Antilles: isotopic and trace element constraints. *Journal of Geophysical Research* **91**, 5927–5941.

Wright, T. L. & Doherty, P. C., 1970. A linear programming and least squares computer method for solving petrological mixing problems. *Geological Society of America Bulletin* **81**, 1995–2008.

Wyllie, P. J., Huang, W-L., Stern, C. R. & Maaloe, S., 1976. Granitic magmas: possible and impossible sources, water contents, and crystallization sequences. *Canadian Journal of Earth Sciences* **13**, 1007–1019.

RECEIVED 22 JULY, 1994
REVISED TYPESCRIPT ACCEPTED 7 JULY, 1995

Downloaded from https://academic.oup.com/petrology/article/37/1/117/1530492 by guest on 21 August 2022